


## Hadronic structure on the light front. II. QCD strings, Wilson lines, and potentials

Edward Shuryak<sup>\*</sup> and Ismail Zahed<sup>†</sup>

Center for Nuclear Theory, Department of Physics and Astronomy, Stony Brook University,  
Stony Brook, New York 11794–3800, USA

 (Received 17 August 2022; accepted 12 January 2023; published 24 February 2023)

This is the second paper on hadronic wave functions in the light-front formulation. We first consider only confinement effects, using the classical Nambu-Gotto string with massive end points in the light-cone gauge. We derive the light-front Hamiltonian and show how to solve it, using an expansion in suitable basis functions. We next discuss the correlators of Wilson lines on the light front, leading to an effective Hamiltonian that includes spin effects. At the end, we consider a separate problem of instanton-induced interactions, at the origin of the pion as a massless Goldstone mode on the light front.

DOI: [10.1103/PhysRevD.107.034024](https://doi.org/10.1103/PhysRevD.107.034024)

### I. INTRODUCTION

The physics of hadrons is firmly based in quantum chromodynamics, a theory over half a century old. One might think that by now this subject has reached a solid degree of maturity with most issues settled. Yet persisting tension remains between the nonperturbative aspects of the theory and empirical measurements using inclusive and exclusive processes.

More specifically, first principle approaches—lattice and semiclassical—are focused on the ground state properties of the QCD vacuum, both using an Euclidean time formulation. Hadrons are then studied via certain correlation functions. However, a significant part of the experimental information—parton distribution functions (PDFs) used in deep inelastic inclusive processes, and distribution amplitudes (DAs) used for exclusive processes—are defined using light-front kinematics, and therefore are not directly accessible by the Euclidean formulation. Only recently, the first attempt to formulate the appropriate kinematical limits [1] and use the lattice for calculating the PDFs and PDAs [2,3] were carried out with some success.

Bringing the two sides of hadronic physics together is not just a technical issue related with kinematics. Even the main pillars of the theory—confinement and chiral symmetry breaking—become contentious. In particular, 60 years ago Nambu and Jona-Lasinio (NJL) [4] have

explained that pions are light because they are near-massless vacuum waves due to the spontaneous breaking of chiral symmetry. The mechanism creating the vacuum quark condensate and the ensuing organization using chiral perturbation theory have since been discussed and confirmed in countless papers. More importantly, the QCD vacuum characteristics in the mesoscopic limit reveal multi-quark correlations captured by universal spectral fluctuations in the zero mode zone (ZMZ) [5], analogous to the universal conductance fluctuations around the Fermi surface in dirty metals [6], an unambiguous signature of the topological nature of the spontaneous breaking of chiral symmetry. And yet, parton dynamics is still treated as if the vacuum is “empty” and quark-partons massless. There were even suggestions that on the light front there are no condensates [7,8], although recently these arguments were revisited [9]. Pions were also argued to be massless due to other reasons [10].

Another serious gap between hadron spectroscopy in the rest frame and on the light front is due to the complex and dynamical nature of the relativistic boost operator: what can be a static potential in one frame, can well become partons on the light front. But even more striking is the difference in the very logical structure of the theory. In the rest frame spectroscopists start from certain Hamiltonians and derive the wave functions, like in atomic or nuclear physics. On the light front, phenomenologists mostly deal with parton distribution functions or distribution amplitudes, matrix elements of the density matrices or the wave functions obtained from experiment or lattice simulations. Few considerations of the light-front Hamiltonians and wave functions are mostly guessed rather than derived.

The aim of this work is to derive the light-front Hamiltonian and the corresponding wave functions (LFWFs), starting with the most basic meson settings

<sup>\*</sup>edward.shuryak@stonybrook.edu

<sup>†</sup>ismail.zahed@stonybrook.edu

Published by the American Physical Society under the terms of the [Creative Commons Attribution 4.0 International license](https://creativecommons.org/licenses/by/4.0/). Further distribution of this work must maintain attribution to the author(s) and the published article's title, journal citation, and DOI. Funded by SCOAP<sup>3</sup>.

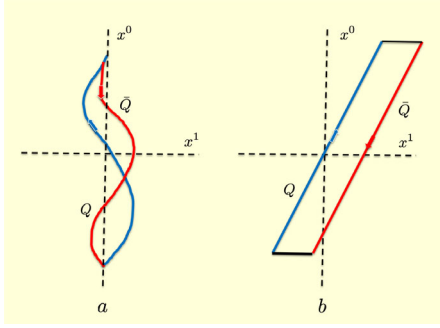


FIG. 1.  $\bar{Q}Q$  meson in the rest frame (a) and in the light-front frame (b).

and certain nonperturbative dynamics. In this methodical paper we will focus on “the main components” of the wave functions with zero orbital momentum, and ignore different spin structures. Its generalization to full wave functions, with all allowed spin and angular momentum values, will be done in the next papers of the series [11–13].

One Hamiltonian leads to an infinite set of wave functions, any of which have infinitely many matrix elements. LFWFs are mutually orthogonal and can be properly normalized. The DAs are normalized only to certain empirical constants, like  $f_\pi$  for a pion. The PDFs of baryons are traced over all quarks but the struck one: tracing mixes together all sectors of the wave function, with different quantum numbers and even the number of partons. Due to quantum entanglement, it leads to a nonzero entropy.

Deriving these Hamiltonians and solving for LFWFs is not an easy task, but going to light front offers certain theoretical advantages. In conventional spectroscopy it is much easier to follow nonrelativistic heavy quarkonia which are moving slowly. Central and spin-dependent forces among them can be formulated in terms of certain universal (flavor-independent) correlators of background fields, which can be evaluated on the lattice or semiclassically (as we tried to do). Light quarks are involved in complicated quantum motion, as depicted in the left sketch in Fig. 1. Usage of nonrelativistic kinetic energy and potentials, as we did in Paper I [14], is qualitative at best.

However, it is improved in the LF frame, as the motion of all quarks gets “frozen” (see the right sketch), the distinctions between the heavy and the light quarks basically go away, as both can be “eikonalized” and treated in fully relativistic formalism. If so, their interactions can be deduced from pertinent Wilson line correlators for any quark mass.

### A. Light-front wave functions

Light-front quantization has a long history with fundamental formulations in QED, atomic and nuclear physics, which we will not review here. Instead, we will comment on a recent revival of its use in the context of hadronic physics. More specifically, we will make use of the

methodical framework in terms of a transverse oscillator basis as discussed by Jia and Vary [15,16]. Their postulated Hamiltonian has led to the light-cone wave functions for the pions and rho mesons, which was shown to be in agreement with a number of experimental results. We will return to its discussion in Sec. IV.

This approach has been extended to the three- and five-quark baryonic sectors by one of us [17], addressing the well-known puzzle of the isospin asymmetry of the “antiquark sea.” Currently this approach has developed into two lines of research. One continues to use the Jia-Vary Hamiltonian with a NJL residual interaction, while the other (called Basis Light Front Quantization BLFQ collaboration) [18] trades the NJL interaction with an effective (massive) gluon, and focuses on the two meson components,  $\bar{q}q$  and  $\bar{q}qg$ .

In yet another important theory development, Brodsky and collaborators [19] have pointed to the similarities between the QCD light-front quantization for a two-particle system and the “soft wall AdS/QCD” holographic model [20] for mesons, which elegantly reproduces the Regge dependence on the radial  $n$  quantum number of the squared hadronic masses  $M^2 \sim n$ , via quantization through the extra holographic coordinate  $z$ . A special role was proposed to the “zeta” combination of the transverse coordinate  $b_\perp$  and the longitudinal momentum fraction  $x$ , which for mesons is

$$\zeta \equiv b_\perp \sqrt{x(1-x)}. \quad (1)$$

It has been suggested that on the light front it plays the same role as the radial coordinate  $r$  in nonrelativistic quantum mechanics in the rest frame. In other words, the LFWF wave function is approximated by a function of this combination only,  $\psi(\zeta)$ .

Furthermore, zeta has been identified with the holographic coordinate  $z$  and, on this basis, the corresponding Schrödinger equation was proposed to have the form

$$\left( -\frac{d^2}{d\zeta^2} - \frac{1-4L^2}{4\zeta^2} + U(\zeta) \right) \psi(\zeta) = M^2 \psi(\zeta) \quad (2)$$

with the quadratic potential  $U = \kappa^4 \zeta^2 + 2\kappa^2(J-1)$ , as for the soft wall AdS/QCD. A similar correspondence was also proposed for baryons, with a “generalized”  $\zeta$  and a corresponding equation, with a kind of “supersymmetry” between mesons and baryons. A physics basis for such approximation is approximate constituent quark-scalar diquark symmetry, suggested in our work [21].

While these works have unquestionably contributed to the rapid and analytic progress in the field over the past decade, we think it is time to proceed more cautiously, and derive all basic quantities systematically, starting from well-established empirical and theoretical facts. We will analyze the accuracy of the approximations made, using certain basic examples, focusing on the internal consistency

and agreement with the wider set of data, e.g. Regge phenomenology for principle quantum number  $n$  and angular momentum  $J$ .

### B. The structure of the paper

The first problem we address is a basic meson problem with linear confinement. In Sec. III we will derive the light-cone Hamiltonian following from the Nambu-Gotto string with massive ends as a model for a relativistic bound meson by a relativistic string with constitutive quark masses. We will first discuss the Hamiltonian in  $1 + 1$  dimensions and show that its diagonalization leads to the famed 't Hooft equation. We will then proceed to  $1 + 3$  dimensions and derive the corresponding squared mass operator for a relativistic bound meson, which turns out to be iterative and nonlocal. In the heavy quark mass limit, we use the semiclassical approximation to detail the heavy meson spectrum. In general, the iterative and nonlocal aspect of the squared mass operator can be simplified, using the einbein trick and minimization, modulo normal ordering.

The solution of this problem can be done by numerical diagonalization in a suitable basis. The results obtained for the masses and LFWFs compare favorably with those obtained in the rest frame for the spectrum of the same model. In Sec. IV we discuss other light-front Hamiltonians suggested in the literature.

In Paper I [14] we discussed mesons, in the center-of-mass (CM) frame. In this case the central (and spin-dependent) potentials are derived from nonlocal correlators of parallel Wilson lines (and lines with extra field strengths). We used a certain instanton-based model of the vacuum to evaluate those, and to relate these potentials and resulting spectra to the mesonic phenomenology. In Sec. V we show how instantons in the vacuum contribute to the parallel Wilson lines for the nonzero quark modes in a boosted meson on the light front. The nonzero mode contributions through vacuum tunneling, as captured by the spin-flavor dependent 't Hooft interaction, are discussed in Sec. IX. In Sec. X we show how the pion emerges on the light cone in the chiral limit with a finite constituent quark mass. The deviation from the chiral limit is in agreement with the Gell-Mann-Oakes-Renner (GOR) relation for the mass. Our conclusions and their discussion are in Sec. XI.

## II. CONFINEMENT IN THE BASIC RELATIVISTIC MESON PROBLEM

In the first paper of this series [14], we focused on the origin of the central and spin-dependent potentials in CM frame. In particular, we detailed the lowest states, and used the nonrelativistic Schrödinger equation not only for heavy quarkonia but for light mesons as well. Now, before we move to the light-front quantization, we will discuss a *basic* relativistic problem of two massive particles connected by a classical string, generating a linear confining potential.

We will also discuss not only the low but also high mass excitations.

It is well known from phenomenology that the excited mesons (as well as baryons) form certain Regge trajectories, relating their masses  $M_J$  to angular momentum  $J$ . For mesons made of light quarks they are close to linear

$$J = a_M + \alpha' M_J^2, \quad (3)$$

where  $a_M$  is called the *intercept* and  $\alpha'$  is called the *slope* of the trajectory, related to the string tension  $\alpha' = 1/2\pi\sigma_T$ . For mesons containing heavy quarks, the trajectories are curved. A thorough discussion of a *classical* model consisting of two rotating masses connected by a string is made in [22], which also provides accurate Regge-style fits to a number of light and heavy mesons.

In this work we rather focus on the *radial* excitations of the light mesons, and consider the relation between the (squared) masses  $M_n^2$  and the radial quantum number  $n$ . For that, consider the reduced or *half* of the system in question, with one quark of mass  $m_Q$ , and half the string. Classically, the energy is a sum of kinetic and potential

$$E = V(r) + \sqrt{\vec{p}^2 + m_Q^2} \quad (4)$$

or

$$(E - V(r))^2 = \vec{p}^2 + m_Q^2. \quad (5)$$

To quantize it, we use the standard substitution of the squared momentum

$$\vec{p}^2 \rightarrow -\frac{\partial^2}{\partial r^2} - \frac{2}{r} \frac{\partial}{\partial r} + \frac{\hat{J}^2}{r^2}$$

with the radial Laplacian (the first two terms) and the angular Laplacian substituted by angular momentum  $\hat{J}^2$ . However, the proper quantization of such a relativistic Klein-Gordon equation is not as simple as the nonrelativistic Schrödinger equation. In particular, if one just takes the linear form of the potential  $V(r) = \sigma_H r$ , the problem is identical to that of a constant electric field, in which particle production takes place through the Schwinger mechanism (Klein paradox), and states with fixed particle number do not, strictly speaking, exist. We will return to the discussion of this equation in Appendix A, and here we will use its semiclassical treatment by the WKB approximation only.

Generically, we have a *turning point*  $p(r_*) = 0$ : note that dynamics is different for  $r < r_*$  and  $r > r_*$ . For simplicity, let us start with the massless case  $m = 0$ , in which  $E_n - \sigma_T r_* = 0$ , and  $r < r_*$  where the momentum is real, and the standard WKB approach can be applied in its original form due to Bohr

$$n\hbar = 4 \int_0^{r_*} p(r, E_n) dr \quad (6)$$

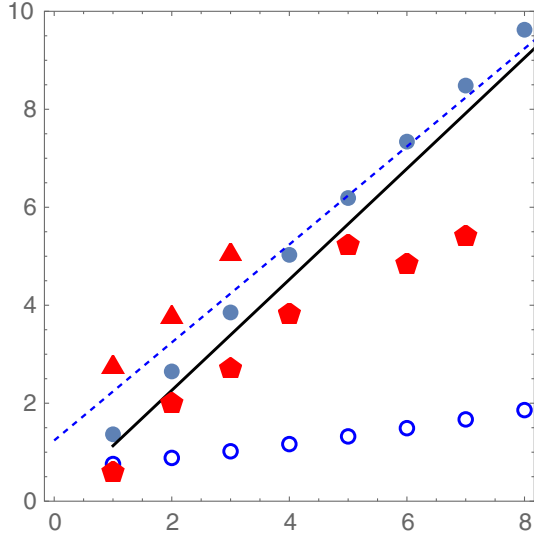


FIG. 2. The squared masses of the  $n + 1$ th states  $E_{n+1}^2$  (GeV<sup>2</sup>) versus the radial quantum number  $n + 1$ . The closed points are for constituent quarks with mass 0.35 GeV. The solid line corresponds to the massless limit with  $E_{n+1}^2 = (n + 1/2)/\alpha'$ . The red five-polygons are the experimental data for the  $\omega$  mesons, and the red triangles are for the  $\omega_3$  mesons listed in the PDG. The open points show the corresponding values from the Jia-Vary confining Hamiltonian (39), with their recommended value  $\kappa = 0.227$  GeV. The dashed line corresponds to the same expression with  $\kappa = 0.5$  GeV.

(here 4 appears as the integral covers a quarter of the period).

For  $J = 0$  and the linear potential  $V = \sigma_T r$ , this can be analytically calculated; the result takes the form

$$n = a_M + \alpha' E_n^2 \left[ \sqrt{1 - b^2} + b^2 \log \left( \frac{1 - \sqrt{1 - b^2}}{b} \right) \right], \quad (7)$$

where the ‘‘Reggeon slope’’ is  $\alpha' = 1/2\pi\sigma_T$ . For two particles  $E_n$  is the total energy of both, and  $b = 2m_Q/E_n$ . Here we added a parameter  $a_M$ , known as a ‘‘quantum shift,’’ which is not well determined. In [22] it is used as a free parameter, different for different Regge trajectories. We will use the standard WKB recipe taking  $a_M = 1/2$ : as shown in [22], this value is correct for all light vector mesons  $\rho, \omega, K^*, \phi$ , but takes different values for other channels. Of course, confinement is not the only term of the Hamiltonian, and shifts are expected. All vector mesons we will use seem to have such ‘‘residual interactions’’ to be minimal. They are likely due to spin forces as we will detail below.

For arbitrary masses, the right-hand side of (7) is a complicated function of energy  $E_n$ , which cannot be inverted analytically. Instead of using some approximate formulas, we inverted it numerically. In Fig. 2 the closed points correspond to the squared masses of the radial excitations (in GeV<sup>2</sup>) with  $n + 1 = 1-10$ , for a constituent

quark mass  $m_Q = 0.35$  GeV and a string tension  $\sigma_T = (0.42 \text{ GeV})^2$ . The results are not far from the asymptotic massless formula shown by the thick straight line, so the mass corrections are small. For heavier quarks, the deviations are larger and the trajectory becomes somewhat curved, as we also suggest below.

The red points represent the experimental data, from which we selected two sets of mesons, namely  $\omega$  ( $J = 1, l = 0$ ) and  $\omega_3$  ( $J = 3, l = 2$ ). Note first that the numerical value of the string tension, obtained from the quarkonium spectra we use, also fits the slope of the Regge trajectories quite accurately.

Note also that if one moves the  $\omega_3$  points to the right by two units, they would nearly coincide with the  $\omega$  data points: this means that the popular assumption that radial quantum number  $n$  and orbital momentum  $l$  appear as a simple sum,  $n + l$ , is approximately correct. However, in general we do not see why this assumption should be accurate for massive quarks, and plotted them without such shift. Still, it is important that the vertical splitting  $M^2(\omega_3) - M^2(\omega)$  is approximately independent of  $n$ . In the subsequent sections it would be ascribed to two quanta of excitation of the transverse oscillator.

### III. CONFINEMENT ON THE LIGHT FRONT

The challenges of the light-front formulation are well known. A direct boost of the Hamiltonian and wave functions from the rest frame must involve both the Hamiltonian and the momentum operators, which are difficult to achieve. Still, one can compare certain boost-independent quantities—excitation masses and transverse momenta.

#### A. Confinement in 1+1 dimensions

As we already mentioned, chiral symmetry breaking basically solves the ‘‘mass problem,’’ giving rise to a constituent quark mass  $m_Q \sim 0.35$  GeV. In the timelike gauge  $x^0 = \tau$ , the free Hamiltonian containing these masses is

$$H \equiv P^0 = p_q^0 + p_{\bar{q}}^0 = (\vec{p}_q^2 + m_Q^2)^{\frac{1}{2}} + (\vec{p}_{\bar{q}}^2 + m_Q^2)^{\frac{1}{2}} \quad (8)$$

which is the expected result for relativistically moving end points. In the light-cone gauge  $x^+ = (x^0 + x^1)/\sqrt{2} = \tau$ , the on-shell relation reads  $2p_{q,\bar{q}}^+ p_{q,\bar{q}}^- = m_Q^2$ . The free light-cone Hamiltonian is then

$$H \equiv P^- = p_q^- + p_{\bar{q}}^- = \frac{m_Q^2 + \vec{p}_{q\perp}^2}{2p_q^+} + \frac{m_Q^2 + \vec{p}_{\bar{q}\perp}^2}{2p_{\bar{q}}^+} \quad (9)$$

Confinement is produced by the so-called QCD strings (electric flux tubes) with a string tension  $\sigma_T \approx (420 \text{ MeV})^2 \sim 1 \text{ GeV/fm}$ . For sufficiently long strings, their world-sheet dynamics is captured by the classical and universal Nambu-Gotto action



$$S_P[x] \approx \sigma_T \int_0^T d\tau \int_0^\pi d\sigma \sqrt{(\dot{x} \cdot x')^2 - \dot{x}^2 x'^2} + m_Q \int_0^T d\tau \left( \sqrt{\dot{x}^2(\tau, 0)} + \sqrt{\dot{x}^2(\tau, \pi)} \right) \quad (10)$$

with  $x^\mu(\tau, \sigma)$  the string coordinate. The last term represents the massive end points, and for simplicity we set the masses equal with  $m_Q = m_{\bar{Q}}$ . Without the string, the end points carry momenta  $p_{q,\bar{q}}^\alpha = m_Q \dot{x}_{q,\bar{q}}^\alpha / |\dot{x}_{q,\bar{q}}|$  with  $p_{q,\bar{q}}^2 = m_Q^2$ . The addition of the string will change the energy, momentum, and angular momentum of the  $\bar{Q}Q$  pair, as we now detail.

As a warmup, consider first the simpler case where the string is embedded in 1 + 1 dimensions and ignore the transverse directions. Equation (10) readily leads to [23,24]

$$H \equiv P^- = \frac{m_Q^2}{2p_q^+} + \frac{m_Q^2}{2p_{\bar{q}}^+} + \sigma_T |x_{\bar{q}}^- - x_q^-|. \quad (11)$$

Using the CM  $R = (x_q^- + x_{\bar{q}}^-)/2$  and relative coordinate  $r = (x_{\bar{q}}^- - x_q^-)$ , and their corresponding momenta  $P^+ = (p_q^+ + p_{\bar{q}}^+)$  and  $k^+ = (p_q^+ - p_{\bar{q}}^+)/2$ , the light-cone Hamiltonian (11) yields the squared meson mass operator

$$M^2 = 2P^+P^- = 2P^+ \left( \frac{2m_Q^2P^+}{P^{+2} - 4k^{+2}} + \sigma_T |r| \right) = \frac{m_Q^2}{\frac{1}{4} - \xi^2} + 2\sigma_T |P^+ r| \quad (12)$$

with the Bjorken  $\xi = k^+/P^+ = \frac{1}{2} + x$  for the fraction of relative momentum carried by the quark at the end point, and  $|\xi| \leq \frac{1}{2}$  or  $0 \leq x \leq 1$ . Since  $k^+$  is canonically conjugate to the relative end-point lightlike coordinate  $r$  or  $[r, k^+] = i$ , we can either use the  $k$  or  $r$  representation for the squared mass. In the  $k$  representation with fixed Bjorken  $x$ , the coordinate is then the operator  $r = id/dk^+$  and the squared mass Hamiltonian (12) reads

$$M^2 = 2P^+P^- = \frac{m_Q^2}{x\bar{x}} + 2\sigma_T |id/dx| \quad (13)$$

with  $\bar{x} \equiv 1 - x$ .

The meson LFWFs and masses follow by diagonalizing (13)

$$\left( \frac{m_Q^2}{x\bar{x}} + 2\sigma_T |id/dx| \right) \varphi_n(x) = M_n^2 \varphi_n(x) \quad (14)$$

which can be rewritten in the 't Hooft equation form [25]

$$M_n^2 \varphi_n(x) = \frac{m_Q^2}{x\bar{x}} \varphi_n(x) - \frac{2\sigma_T}{\pi} \text{PV} \int_0^1 dy \frac{\varphi_n(y) - \varphi_n(x)}{(x-y)^2} \quad (15)$$

with the identification of the string with the gauge coupling through  $\sigma_T \equiv g^2 N_c / 2$  for QCD in 1 + 1 dimensions, as originally noted in [23,24] in the large number of colors  $N_c$  limit. The two-dimensional confining potential in the Bjorken  $x$  representation is

$$\langle x || id/dx || y \rangle = \int_{-\infty}^{+\infty} \frac{dq}{2\pi} e^{iq(x-y)} |q| \rightarrow \text{PV} \frac{-1}{\pi(x-y)^2} + \frac{-1}{\pi x \bar{x}} \quad (16)$$

using the principal value prescription,

$$\text{PV} \frac{1}{z^2} = \frac{1}{2} \left[ \frac{1}{(z+i0)^2} + \frac{1}{(z-i0)^2} \right]. \quad (17)$$

The induced self-energy which is *negative* in (15)

$$-\frac{2\sigma_T}{\pi} \text{PV} \int_0^1 dy \frac{-\varphi_n(x)}{(x-y)^2} = \frac{-2\sigma_T/\pi}{x\bar{x}} \varphi_n(x) \quad (18)$$

can be made more manifest by recasting the 't Hooft equation (15) in the equivalent form

$$M_n^2 \varphi_n(x) = \frac{m_Q^2 - 2\sigma_T/\pi}{x\bar{x}} \varphi_n(x) - \frac{2\sigma_T}{\pi} \text{PV} \int_0^1 dy \frac{\varphi_n(y)}{(x-y)^2}. \quad (19)$$

The spectrum following from (19) admits a massless mode  $\varphi_0(x) \rightarrow \theta(x\bar{x})$ , provided that the *current quark mass*  $m_Q \rightarrow 0$ . (The constituent quark mass in QCD in 1 + 1 dimensions is gauge dependent and divergent.) The *positive* string pair interaction balances the induced Coulomb self-energy which is *negative*. In QCD in 1 + 1 dimensions, the massless mode appears only in the large number of colors limit owing to the Berezinskii-Kosterlitz-Thouless mechanism. In massless QCD in 1 + 3 dimensions, the pion is a true Nambu-Goldstone mode.

The semiclassical spectrum following from (15) Reggeizes with a mass gap

$$\int_{x_-}^{x_+} dx \left( M_n^2 - \frac{m_Q^2}{x\bar{x}} \right) = M_n^2 - m_Q^2 \ln \left( \frac{x_+ \bar{x}_-}{x_- \bar{x}_+} \right) = 2\pi\sigma_T n \quad (20)$$

with the turning points

$$x_\pm = \frac{1}{2} \left( 1 \pm \left( 1 - \frac{4m_Q^2}{M_n^2} \right)^{\frac{1}{2}} \right) \quad (21)$$

and with  $M_n \geq 2m_Q$ . The mass gap vanishes for  $m_Q \rightarrow 0$  with a radial Regge trajectory  $M_n^2 = n/\alpha'$ , and  $\alpha' = 1/2\pi\sigma_T$  the slope of the open bosonic string as it should. At large  $n$ , the 't Hooft equation (15) can be solved semiclassically giving the light-cone wave functions  $\varphi_n(x) \approx \sqrt{2} \sin((n+1)\pi x)$  [25]. In the massive case, the Regge trajectory is modified to  $M_n^2 \approx n/\alpha' + 2m_Q^2 \ln n$ .

### B. Light-front Hamiltonian for a string in 1+3 dimensions

We now return to our main problem, the mesonic Hamiltonian and wave functions on the light front. We use the string (10) in the light-cone gauge in 1+3 dimensions. Ignoring the string vibrations (Luscher term and its corrections in higher order) the result can be read off from (13)

$$M^2 = 2P^+P^- = \frac{m_Q^2 + k_\perp^2}{x\bar{x}} + 2\sigma_T \left( |id/dx|^2 + \frac{P^{+2}x_\perp^2}{\gamma^2} \right)^{\frac{1}{2}} \quad (22)$$

with the Lorentz factor  $\gamma = P^+/Mv \rightarrow \infty$  as  $v \rightarrow c$  gets close to the light cone,

$$M^2 = 2P^+P^- = \frac{m_Q^2 + k_\perp^2}{x\bar{x}} + 2\sigma_T (|id/dx|^2 + M^2x_\perp^2)^{\frac{1}{2}} \quad (23)$$

Again, the transverse coordinate and momenta  $x_\perp, k_\perp$  are conjugate and (for fixed Bjorken  $x$ ) it is appropriate to use  $\vec{x}_\perp = i\vec{\nabla}_\perp$  to diagonalize the squared mass operator in full momentum representation. The generalization of (13) in 1+1 dimensions to (23) in 1+3 dimensions was also noted in [26].

The squared mass operator (Hamiltonian) is now given in terms of a nonlinear differential operator. It is a symbolic form since one still has to define certain procedures for calculating its matrix elements, which can be done only *modulo ordering ambiguities*. A good test for these procedures is provided by a requirement that the mass spectrum be the same as in the CM frame. In particular, the semiclassical spectrum should “Reggeize” to  $M_{nl}^2 \approx 2\pi\sigma_T(n+l)$  for the  $n$ -radial and  $l$ -orbital excitations.

Another issue is that  $M^2$  appears not only in the left-hand side of (23) but also in the right-hand side. For *heavy* mesons on the light cone, one can assume  $M \approx 2m_Q$  on the right-hand side,

$$M_H^2 \approx \frac{m_Q^2 + k_\perp^2}{x\bar{x}} + 2\sigma_T (|id/dx|^2 + (2m_Q)^2x_\perp^2)^{\frac{1}{2}} \quad (24)$$

and avoid the iterative process. Furthermore, in the heavy-quark limit,  $x \approx \bar{x} \approx \frac{1}{2}$  and (24) simplifies to

$$M_H^2 \approx (2m_Q)^2 + 4k_\perp^2 + 4m_Q\sigma_T|x_\perp|. \quad (25)$$

Note that the effective string tension is now growing with  $m_Q$ . This is reasonable, since the binding energy for a slowly moving but heavy quark should compensate its kinetic energy  $m_Q v_Q^2/2$ , which depends on  $m_Q$ . The semiclassical spectrum follows from

$$\int_{\rho_-}^{\rho_+} d\rho \left( M_{H,nl}^2 - (2m_Q)^2 - \frac{4l^2}{\rho^2} - 4m_Q\sigma_T\rho \right)^{\frac{1}{2}} = 2\pi n \quad (26)$$

with the turning points  $\rho_\pm$  fixed by the positive and real solutions to the cubic equation

$$M_{H,nl}^2 = (2m_Q)^2 + \frac{4l^2}{\rho_\pm^2} + 4m_Q\sigma_T\rho_\pm \quad (27)$$

which exists for

$$M_H^2 \geq (2m_Q)^2 + 8(lm_Q\sigma_T)^{\frac{2}{3}}. \quad (28)$$

For  $l=0$ , the radial excitations follow:

$$M_{H,n0}^2 \approx (2m_Q)^2 + \left( \frac{6m_Q}{\alpha'} \right)^{\frac{2}{3}} n^{\frac{2}{3}} \quad (29)$$

with again, the open string Regge slope  $\alpha' = 1/2\pi\sigma_T$ . As we noted earlier, the Regge trajectory is now bent. The heavier  $m_Q$ , the more bound the Regge spectrum. Equation (24) applies also to heavy-light mesons modulo minor changes for asymmetric masses.

Returning to light-light mesons, we note that the non-relativistic approximation  $M \approx 2m_Q$  may still be semi-quantitatively suited for the “ordinary mesons” (like vectors  $\phi, \rho$ ) but not the Nambu-Golstone pseudoscalars. In order to reproduce the mesonic spectra correctly, (23) needs to be supplemented by the spin and flavor-dependent interactions, as we will discuss later.

Finally, we note that if the constituent mass  $m_Q \rightarrow 0$ , (23) admits a non-normalizable massless solution  $\varphi_0(x, b_\perp) \sim \theta(x\bar{x})$  for  $x\bar{x} \neq 0$  since

$$[M^2]_{m_Q=0}\varphi_0(x, k_\perp) = \left[ \frac{k_\perp^2}{x\bar{x}} + 2\sigma_T|id/dx| \right] \theta(x\bar{x}) = 0. \quad (30)$$

At  $x=0, 1$  it vanishes as a power proportional to the mass  $(x\bar{x})^{\#m_Q}$ . This is the same massless solution in the 1+1 dimensional 't Hooft equation (15) as the would-be pion emerges as a massless mode in the chiral limit at large  $N_c$  only if  $m_Q=0$  is identified with the current quark mass. However, this kinematical solution is not the physical pion, since for the latter  $m_Q \neq 0$  is identified with the constituent mass, and does not vanish in the chiral limit.

### C. Eliminating the square root in the Hamiltonian

The inconvenient square root of the differential operator can be avoided by the “einbein trick.” With this in mind, consider the operator

$$M^2(a, b) = \frac{m_Q^2 + k_\perp^2}{x\bar{x}} + \sigma_T \left( \frac{|id/dx|^2 + bx_\perp^2}{a} + a \right) \quad (31)$$

with the auxillary parameters  $a$  (inverse einbein  $a = 1/e$ ) and  $b$ . Note that minimization over  $a$  would return us to the original Hamiltonian with the square root: but we

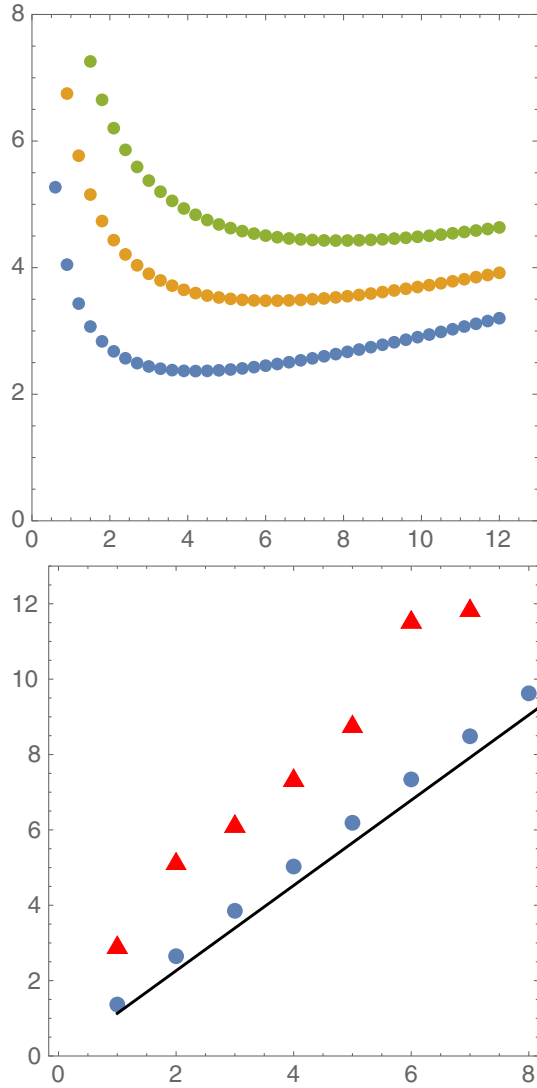


FIG. 3. The upper plot shows the dependence of the three lowest eigenvalues  $M_n^2$  on the parameter  $a$ , in the region around their minima. The lower plot shows  $M_{n+1}^2$  versus  $n+1 = 1 \dots 7$ . The results obtained from the Hamiltonian diagonalization with fixed  $a = 2.36$  are shown by red triangles. The blue disks are the semiclassical results discussed previously, the line is a simple linear expression  $M_n^2 = n/\alpha'$ , both shown for comparison.

will do minimization in  $a$  afterwards, after diagonalization. The parameter  $b$  would be iteratively selected to reach self-consistency when  $b \rightarrow M_{nl}^2$ . (Strictly speaking  $b$  is originally  $M^2$ , so the minimization in  $a$  is more subtle.

This subtlety will be ignored for now, as well as the ordering issue we pointed out.)

Let us represent this Hamiltonian as a sum of two terms,  $M^2 \equiv H_0 + V$ ,

$$H_0 = \frac{\sigma_T}{a} \left( -\frac{\partial^2}{\partial x^2} - b \frac{\partial^2}{\partial k_\perp^2} \right) + \sigma_T a + 4(m_Q^2 + k_\perp^2). \quad (32)$$

Note that the last term is artificially added; it is then subtracted from the “potential” defined by

$$V(x, \vec{k}_\perp) \equiv (m_Q^2 + k_\perp^2) \left( \frac{1}{x\bar{x}} - 4 \right). \quad (33)$$

Eigenstates of  $H_0$  provide the functional basis set described in Appendix B. The Hamiltonian  $M^2$  consists of the diagonal part  $H_0$ , and nondiagonal “potential”  $V$  part. In the orthonormal set of functions defined in Appendix B,  $M^2$  is represented by (infinite) matrices, with its  $12 \times 12$  part given explicitly.

For the simple “bare mass approximation” with the parameter  $b = (2m_Q)^2$ , one can diagonalize the (part of the) Hamiltonian. The dependence of the (three lowest) eigenvalues on the parameter  $a$  is shown in the upper plot of Fig. 3. There are clear minima as a function of  $a$ . While they do not happen to be at the same values, the dependence  $M_n^2(a)$  is relatively minor, and selecting a certain compromise value gives reasonable numerical accuracy. We use  $a = 2.36$  (a minimum for the lowest  $n = 1$  state).

With the parameters  $a, b$  fixed, the Hamiltonian becomes a numerical matrix, which can be readily diagonalized. Keeping the  $12 \times 12$  part of the matrix, we obtain the 12 eigenvalues shown in the lower part of Fig. 3 (red triangles). For comparison we also show the semiclassical results. The Regge slope is well reproduced, while the intercept  $a_M$  is not. This can be attributed to the fact that our LF Hamiltonian includes zero mode oscillation energy in all three directions, missing in the semiclassical treatment.

In principle, one may tune the parameters  $a, b$  for each state separately, to reach agreement for the masses. However, this would mean that different states are not eigenstates of the same Hamiltonian, and therefore not mutually orthogonal. Instead of doing that, we keep the  $a, b$  values the same for all considered states, and look at the main object of our interest, the derived wave functions. For example, in the approximation considered, the lowest state has the following LFWF:

$$\begin{aligned} \psi_1(\rho, x) = & \beta e^{-\beta^2 \rho^2 / 2} \left( (0.831 - 0.0371\beta^2 \rho^2 + 0.00100\beta^4 \rho^4) \sin(\pi x) \right. \\ & + (-0.0252 - 0.0107\beta^2 \rho^2 + 0.000566\beta^4 \rho^4) \sin(3\pi x) \\ & + (-0.00427 - 0.00207\beta^2 \rho^2 + 0.000168\beta^4 \rho^4) \sin(5\pi x) \\ & \left. + (-0.00145 - 0.000743\beta^2 \rho^2 + 0.0000633\beta^4 \rho^4) \sin(7\pi x) \right). \end{aligned} \quad (34)$$

We recall that here  $\rho = p_\perp$ , and the oscillator parameter is  $\beta = (4a/\sigma_T b)^{\frac{1}{2}}$ .

Note that only the first coefficient (0.831) is large, while the others are at few percent level or smaller. If plotted, the Gaussian curve is hard to separate from the full expression. This means that the main  $p_\perp$  dependence is mostly Gaussian, while the  $x$  dependence is nearly  $\sim \sin(\pi x)$  (amusingly as in 1+1 dimensions). This is explained by our definition of the oscillator term  $4(m_Q^2 + p_\perp^2)$  (which was added and subtracted), making the nondiagonal matrix elements of the Hamiltonian relatively small. Using the Gaussian approximation for the ground state, the absolute scale of the rms of the transverse momentum is

$$\langle p_\perp^2 \rangle = \frac{1}{\beta^2} = \sqrt{\frac{\sigma_T b}{4a}}. \quad (35)$$

Finally, (31) can be solved in three dimensions  $x, p_x, p_y$  without recourse to the matrix diagonalization. The method

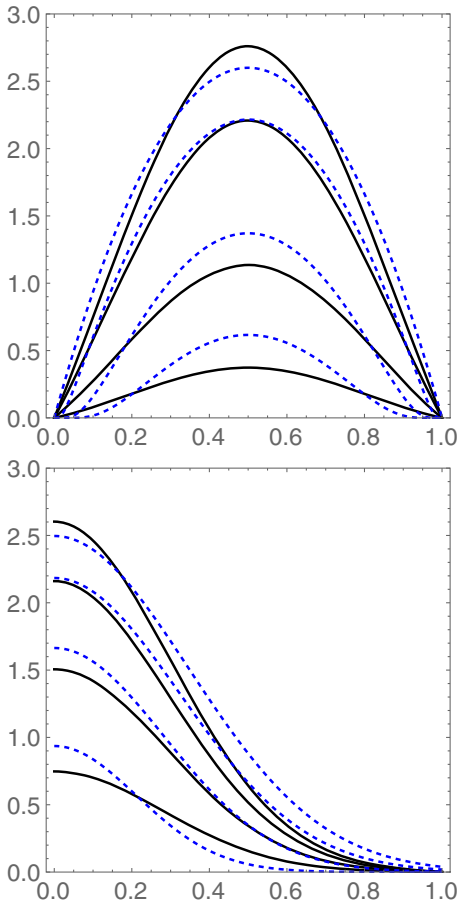


FIG. 4. The upper plot shows the dependence of the ground state wave function  $\Psi_0(x, p_\perp)$  on  $x$  at  $p_\perp^2 = 0, 0.2, 0.4, 0.6$  GeV<sup>2</sup>, top to bottom curves. The lower plot is on  $p_\perp$  at  $x = 0.1, 0.2, 0.3, 0.4$ . All solid curves are from the exact solution, while all dashed lines are for the simplified form (36).

consists of solving directly the partial differential equation, with Dirichlet boundary conditions on the support with Bjorken  $x$ . The ground state eigenvalue is  $M^2 = 2.58$  GeV<sup>2</sup>, in good agreement with the matrix diagonalization. The difference between the numerical solution and (34) is inside the width of the line. No change in the normalization was needed. Orthogonality also works very accurately.

Since we have two solutions, one numerical and one analytical (34), they can be plotted in various ways. One way is to make a comparison to the form suggested in the literature

$$\Psi_0(x, \xi) = 4C_2 x \bar{x} e^{-C_1 \xi^2}, \quad (36)$$

with

$$\xi^2 = \frac{p_\perp^2}{x \bar{x}} \quad (37)$$

the Brodsky-DeTera mond variable. The constants are fixed as  $C_2 = 2.6$ ,  $C_1 = 1$ . The comparison between our exact ground state (34) with a simplified form (36) is shown in Fig. 4. The simplified form (36) with the  $\xi$  variable is qualitatively similar but not very accurate, especially at the end points.

#### IV. OTHER LIGHT-FRONT HAMILTONIANS

The method of writing a Hamiltonian as a large matrix in some convenient basis functions, with its subsequent diagonalization, is widely used in atomic and nuclear physics. Jia and Vary in [16] pioneered such an approach to LFWFs. Their assumed Hamiltonian consists of four terms: (i) the effective quark masses originating from the spontaneous breaking of chiral symmetry ( $H_M$ ); (ii) the longitudinal confinement ( $H_\parallel$ ); (iii) the transverse motion and confinement ( $H_\perp$ ); and last but not least, (iv) the NJL four-quark effective interaction  $H_{NJL}$ , which we will not detail here. More specifically,

$$\begin{aligned} H &= H_M + H_\parallel + H_\perp + H_{NJL}, \\ H_M &= \frac{m_Q^2}{x_1} + \frac{m_{\bar{Q}}^2}{x_2}, \\ H_\parallel &= \frac{\kappa^4}{(m_Q + m_{\bar{Q}})^2} \frac{1}{J(x)} \partial_x J(x) \partial_x, \\ H_\perp &= k_\perp^2 \left( \frac{1}{x_1} + \frac{1}{x_2} \right) + \kappa^4 x_1 x_2 r_\perp^2, \end{aligned} \quad (38)$$

where  $m_{Q, \bar{Q}}$  are the constituent quark and antiquark masses,  $\kappa$  is the confining parameter,  $J(x) = x_1 x_2 = (1-s)^2/4$  is the integration measure, and  $\vec{k}_\perp, \vec{r}_\perp$  are the transverse momentum and coordinate. Note that if the masses are the same, one can simplify



$$\frac{1}{x_1} + \frac{1}{x_2} = \frac{1}{x_1 x_2} = \frac{4}{(1-s^2)}.$$

The matrix element of  $H_M$  lacks the factor of  $(1-s^2)$  normally present in their integration measure.

Note that the confining terms are quadratic (rather than linear) in coordinates, and the transverse and longitudinal parts are additive. Therefore it resembles harmonic oscillators. This simplifies the problem of finding its eigenfunctions. Those are explicitly defined in [16]. We will not explain them here, but just mention that with those the Hamiltonian (other than NJL) is diagonal, and its spectrum is analytic,

$$M_{nml}^2 = (m_Q + m_{\bar{Q}})^2 + 2\kappa^2(2n + |m| + l_L + 3/2) + \frac{\kappa^4}{(m_Q + m_{\bar{Q}})^2} l_L(l_L + 1), \quad (39)$$

where  $n$  is the principal quantum number of the transverse oscillator,  $m$  is the angular momentum helicity [from  $\exp(im\phi)$ ], and  $l_L$  is the index of the longitudinal wave functions (not orbital momentum).

The term  $k_{\perp}^2/x_{\bar{x}}$  is kinematically natural on the light front. We try to separate dependence on the transverse and longitudinal momenta by using a certain expansion in basis functions, in the diagonalization presented above.

Trying to cut through these difficulties (and following Brodsky *et al.*) Jia and Vary proposed to change variables to  $\xi$  as given in (37), and call the offensive term its square. Unfortunately, if this change of variables is to be done explicitly, it would complicate significantly the “kinetic energy” of the problem, producing extra terms which were not included.

Let us now compare this spectrum with that of our “basic problem” discussed above. Note first, that the main linear dependence on the integer quantum numbers  $n$ ,  $m$  is in agreement with the linear Regge trajectories. So qualitatively it is in agreement with the data.

Unfortunately, the particular selection of the parameter  $\kappa = 0.227$  GeV makes the slope of the resulting Regge trajectory much smaller than needed: see the open points in Fig. 2 (for  $m = l = 0$ ). To fix this, one needs a larger value, such as e.g.  $\kappa = 0.5$  GeV as indicated by the dashed line in the same figure.

Another test, using the same Fig. 2, can be made using the  $\omega_3 - \omega$  splitting, corresponding to a change in  $m$  by two units. From the expression above, one finds that it should be  $4\kappa^2 \approx 0.2$  GeV<sup>2</sup> if the recommended value  $\kappa = 0.227$  GeV is used. Experimentally, for the three lowest  $\omega_3, \omega$  states it is  $\approx 1.8$  GeV<sup>2</sup>, nearly an order of magnitude larger.

We conclude that while the description of confinement by a Jia-Vary Hamiltonian is qualitatively correct, leading to a Regge-type behavior, the particularly recommended value of the parameter  $\kappa$  leads to a significant underestimation of the confinement effects. The reason is that their analysis focused on the lowest states—specifically on  $\pi, \rho$  mesons—rather than on Regge phenomenology of the excited states. However (as we detailed in our paper [27])  $\rho$  and especially  $\pi$  mesons are a very special case. Being most compact in size, they are strongly affected by the short-range effects (spin potentials and residual interactions), rather than generic effects of confinement.

## V. CENTRAL POTENTIAL FROM INSTANTONS ON THE LIGHT FRONT

In the first paper of this series [14] we discussed a “dense instanton liquid” model, including both the dilute instanton ensemble of the original ILM, responsible for the disordering of the lowest Dirac eigenstates, as well as the “ $\bar{I}\bar{I}$  molecules” with a larger density. We have shown that such a vacuum model can reproduce *both* the *central* potential  $V_C(r)$  at intermediate distances  $r \sim 0.5$  fm, and the nonperturbative *spin-dependent* forces. We recall that the use of instantons is motivated by the fact that the spin-dependent forces stem from (a nonlocal correlator of) *magnetic* fields.

To evaluate the light-cone Wilson loop in Fig. 1 in the instanton vacuum, we follow our original idea for  $Q\bar{Q}$  scattering in [27]. For that we assign a relative angle  $\theta$  between Wilson lines in Euclidean space, carry the summation and tracing over the ensemble of instantons with fixed density  $N/V_4$ , and then analytically continue the *result* to the light front using the substitution  $\theta = -i\chi$  with  $\chi$  being the rapidity difference of the  $Q\bar{Q}$  beams. The connected loop can be written in terms of traces over individual instantons in leading order in  $N/V_4$ . More explicitly, the connected result exponentiates to

$$\langle \mathbf{W}(\theta, 0_{\perp}) \mathbf{W}^{\dagger}(\theta, b_{\perp}) \rangle_C \approx \exp \left( -2 \times \frac{N}{2N_c V_4} \int d^4 z \text{Tr}_c (\mathbf{1} - \mathbf{W}_I(\theta, 0_{\perp}) \mathbf{W}_I^{\dagger}(\theta, b_{\perp})) \right) \quad (40)$$

with  $\mathbf{W}_I(\theta, b_{\perp})$  the sloped Wilson line running through an instanton at a transverse separation  $b_{\perp}$ . The extra overall factor of 2 in the exponent accounts for the anti-instanton contribution.

**A. Case  $\dot{x} \cdot b_{\perp} = 0$** 

Each sloped Wilson line contributes in singular gauge

$$\mathbf{W}_I(\theta, b_{\perp}) = \cos\left(\pi - \frac{\pi\gamma}{\sqrt{\gamma^2 + \rho^2}}\right) - i\hat{n}^a \tau^a \sin\left(\pi - \frac{\pi\gamma}{\sqrt{\gamma^2 + \rho^2}}\right) \quad (41)$$

with

$$\begin{aligned} n^a &= \eta_{\mu\nu}^a \dot{x}_{\mu}(z - b)_{\nu}, \\ \gamma^2 &= n \cdot n = (z_4 \sin \theta - z_3 \cos \theta)^2 + (z_{\perp} - b_{\perp})^2. \end{aligned} \quad (42)$$

In this first case  $b_{\mu} = (0, b_{\perp}, 0)$ ,  $x_{\mu}(s) = (\cos \theta s, 0_{\perp}, \sin \theta s)$  with  $\dot{x} \cdot b_{\perp} = 0$ . Carrying the color trace and using the new coordinates

$$\begin{aligned} z_{-} &= \sin \theta z_4 - \cos \theta z_3, \\ z_{+} &= \cos \theta z_4 + \sin \theta z_3 \end{aligned} \quad (43)$$

yields the result

$$\begin{aligned} \frac{2N}{N_c V_4} \int dz_{+} dz_{-} dz_{\perp} &\left[ 1 - \cos\left(\frac{\pi\tilde{\gamma}}{\sqrt{\tilde{\gamma}^2 + \rho^2}}\right) \cos\left(\frac{\pi\tilde{\gamma}_{\perp}}{\sqrt{\tilde{\gamma}_{\perp}^2 + \rho^2}}\right) \right. \\ &\left. - \frac{z \cdot b_{\perp} - z_{\perp}^2 - z_{\perp}^2}{\tilde{\gamma} \tilde{\gamma}_{\perp}} \sin\left(\frac{\pi\tilde{\gamma}}{\sqrt{\tilde{\gamma}^2 + \rho^2}}\right) \sin\left(\frac{\pi\tilde{\gamma}_{\perp}}{\sqrt{\tilde{\gamma}_{\perp}^2 + \rho^2}}\right) \right] \end{aligned} \quad (44)$$

with

$$\tilde{\gamma}^2 = z_{-}^2 + (z_{\perp} - b_{\perp})^2, \quad \tilde{\gamma}_{\perp}^2 = z_{-}^2 + z_{\perp}^2. \quad (45)$$

Since (44)–(45) are  $z_{+}$  independent, the result scales with  $Z_E^{+} = \int dz_{+}$

$$\langle \mathbf{W}(\theta, 0_{\perp}) \mathbf{W}^{\dagger}(\theta, b_{\perp}) \rangle_C \approx \exp\left[-Z_E^{+} \left(\frac{4\kappa}{N_c \rho}\right) \mathbf{I}\left(\xi = \frac{b_{\perp}}{\rho}\right)\right] \quad (46)$$

and the dimensionless cylindrical integral

$$\begin{aligned} \mathbf{I}(\xi) &= \int_{-\infty}^{+\infty} dy_{-} \int_0^{\infty} y_{\perp} dy_{\perp} \int_0^{2\pi} \frac{d\phi}{2\pi} \\ &\times \left[ 1 - \cos\left(\frac{\pi y}{\sqrt{y^2 + 1}}\right) \cos\left(\pi \left(\frac{y^2 + \xi^2 + 2\xi y_{\perp} \cos \phi}{y^2 + \xi^2 + 2\xi y_{\perp} \cos \phi + 1}\right)^{\frac{1}{2}}\right) \right. \\ &\left. - \frac{y^2 + \xi y_{\perp} \cos \phi}{(y^2 + \xi^2 + 2\xi y_{\perp} \cos \phi)^{\frac{1}{2}}} \sin\left(\frac{\pi y}{\sqrt{y^2 + 1}}\right) \sin\left(\pi \left(\frac{y^2 + \xi^2 + 2\xi y_{\perp} \cos \phi}{y^2 + \xi^2 + 2\xi y_{\perp} \cos \phi + 1}\right)^{\frac{1}{2}}\right) \right] \end{aligned} \quad (47)$$

with the radial variable  $y^2 = y_{-}^2 + y_{\perp}^2$ . Note that for the temporal Wilson loop or  $\theta = 0$  in our case, a similar integral arises for the static potential between two infinitely heavy  $Q\bar{Q}$  with two major differences: (i) the dimensionless integral involves spherical coordination and a spherical measure, and (ii)  $y_{\perp} \cos \phi \rightarrow y \cos \theta_s$  with  $\theta_s$  the spherical angle.

Although  $\theta$  has dropped out of (46) it is worth noting through (43) that  $Z_E^{+}$  analytically continues to the

transverse light-cone coordinate  $iZ_M^{+}$ . With this in mind, (46) analytically continues to

$$\langle \mathbf{W}(\theta, 0_{\perp}) \mathbf{W}^{\dagger}(\theta, b_{\perp}) \rangle_C \rightarrow \exp\left[-iZ_M^{+} \left(\frac{4\kappa}{N_c \rho}\right) \mathbf{I}\left(\frac{b_{\perp}}{\rho}\right)\right] \quad (48)$$

which allows for the identification of the instanton contribution to the light-cone Hamiltonian

$$P_I^- = \frac{1}{\gamma_\beta} \left( \frac{4\kappa}{N_c \rho} \right) \mathbf{I} \left( \frac{b_\perp}{\rho} \right) \quad (49)$$

with the extra Lorentz factor  $\gamma_\beta = \cosh \chi$  correcting for the missing time-dilatation factor in the exponent in (48). The corresponding instanton contribution to the invariant squared mass is

$$2P^+ P_I^- = 2\gamma_\beta M P_I^- \approx 2M \left( \frac{4\kappa}{N_c \rho} \right) \mathbf{I} \left( \frac{b_\perp}{\rho} \right) \quad (50)$$

in leading order in the packing fraction  $\kappa$ . In the chiral limit with zero current quark masses, the full squared mass (without the confining string) is kinetic plus potential

$$M^2 = \frac{k_\perp^2}{x\bar{x}} + 2P^+ P_I^- \approx \frac{k_\perp^2}{x\bar{x}} + 2M \left( \frac{4\kappa}{N_c \rho} \right) \mathbf{I} \left( \frac{b_\perp}{\rho} \right) \quad (51)$$

which amounts to the mass operator

$$M = \frac{|k_\perp|}{\sqrt{x\bar{x}}} + \left( \frac{4\kappa}{N_c \rho} \right) \mathbf{I} \left( \frac{b_\perp}{\rho} \right) + \mathcal{O}(\kappa^2). \quad (52)$$

For  $\xi = b_\perp/\rho \ll 1$  the transverse potential is harmonic with  $\mathbf{I}(\xi) \approx \alpha \xi^2$ , while for  $\xi = b_\perp/\rho \gg 1$  the transverse potential asymptotes twice the induced self-energy  $\mathbf{I}(\xi) \approx 2\Delta m_Q + C/\xi^p$  with  $p \ll 1$ . Typically, the self-energies on the Wilson lines are small  $\Delta m_Q/m_Q < 1$ .

### B. Case $\dot{x} \cdot b_\perp \neq 0$

In this second case  $b_\mu = (0, b_\perp, b_3)$ ,  $x_\mu(s) = (\cos \theta s, 0_\perp, \sin \theta s)$  with  $\dot{x} \cdot b_\perp \neq 0$ . The analysis follows the same reasoning without a longitudinal component  $b_3$ , with (44) now reading

$$\begin{aligned} & \frac{2N}{N_c V_4} \int dz_+ dz_- dz_\perp \left[ 1 - \cos \left( \frac{\pi \tilde{\gamma}}{\sqrt{\tilde{\gamma}^2 + \rho^2}} \right) \cos \left( \frac{\pi \tilde{\gamma}_\perp}{\sqrt{\tilde{\gamma}_\perp^2 + \rho^2}} \right) \right. \\ & \left. - \frac{z_-^2 + \cos \theta z_- b_3 + z_\perp \cdot (z - b)_\perp}{\tilde{\gamma} \tilde{\gamma}_\perp} \sin \left( \frac{\pi \tilde{\gamma}}{\sqrt{\tilde{\gamma}^2 + \rho^2}} \right) \sin \left( \frac{\pi \tilde{\gamma}_\perp}{\sqrt{\tilde{\gamma}_\perp^2 + \rho^2}} \right) \right] \end{aligned} \quad (53)$$

and

$$\begin{aligned} \tilde{\gamma}^2 &= (z_- + \cos \theta b_3)^2 + (z_\perp - b_\perp)^2, \\ \tilde{\gamma}_\perp^2 &= z_-^2 + z_\perp^2. \end{aligned} \quad (54)$$

We now analytically continue  $\theta \rightarrow -i\chi$  or  $\cos \theta \rightarrow \cosh \chi = \gamma_\beta$ , and  $Z_E^+ \rightarrow iZ_M^+$ , and change to the dimensionless variables  $z_-/\rho \rightarrow z_-$  and  $z_\perp/\rho \rightarrow z_\perp$ . The result for (53) is now

$$iZ_M^+ \frac{2N\rho^3}{N_c V_4} \mathbf{H} \left( \frac{1}{M\rho} \frac{id}{dx}, \frac{b_\perp}{\rho} \right) \quad (55)$$

with the dimensionless integral

$$\begin{aligned} \mathbf{H} \left( \frac{1}{M\rho} \frac{id}{dx}, \xi \right) &= \frac{1}{2\pi} \int dz_- dz_\perp \left[ 1 - \cos \left( \frac{\pi \tilde{\gamma}}{\sqrt{\tilde{\gamma}^2 + 1}} \right) \cos \left( \frac{\pi \tilde{\gamma}_\perp}{\sqrt{\tilde{\gamma}_\perp^2 + 1}} \right) \right. \\ & \left. - \frac{z_-(z_- + id/dx/M\rho) + z_\perp \cdot (z_\perp - \xi_\perp)}{\tilde{\gamma} \tilde{\gamma}_\perp} \sin \left( \frac{\pi \tilde{\gamma}}{\sqrt{\tilde{\gamma}^2 + 1}} \right) \sin \left( \frac{\pi \tilde{\gamma}_\perp}{\sqrt{\tilde{\gamma}_\perp^2 + 1}} \right) \right] \end{aligned} \quad (56)$$

with  $\xi_\perp = b_\perp/\rho$  and  $\xi = |\xi_\perp|$  and

$$\begin{aligned} \tilde{\gamma}^2 &\rightarrow (z_- + id/dx/M\rho)^2 + (z_\perp - \xi_\perp)^2, \\ \tilde{\gamma}_\perp^2 &\rightarrow z_-^2 + z_\perp^2. \end{aligned} \quad (57)$$

The integral in (56) is only a function of the combination

$$\tilde{\xi}_x = ((id/dx/M\rho)^2 + \xi_\perp^2)^{\frac{1}{2}} \equiv \xi_x/\rho \quad (58)$$

with the spherical integral

$$\begin{aligned} \mathbf{H}(\xi_x) = & \int_0^\infty y^2 dy \int_{-1}^{+1} dt \left[ 1 - \cos\left(\frac{\pi y}{\sqrt{y^2+1}}\right) \cos\left(\pi \left(\frac{y^2 + \tilde{\xi}_x^2 + 2\tilde{\xi}_x y t}{y^2 + \tilde{\xi}_x^2 + 2\tilde{\xi}_x y t + 1}\right)^{\frac{1}{2}}\right) \right. \\ & \left. - \frac{y + \tilde{\xi}_x t}{(y^2 + \tilde{\xi}_x^2 + 2\tilde{\xi}_x y t)^{\frac{1}{2}}} \sin\left(\frac{\pi y}{\sqrt{y^2+1}}\right) \sin\left(\pi \left(\frac{y^2 + \tilde{\xi}_x^2 + 2\tilde{\xi}_x y t}{y^2 + \tilde{\xi}_x^2 + 2\tilde{\xi}_x y t + 1}\right)^{\frac{1}{2}}\right) \right]. \end{aligned} \quad (59)$$

The corresponding instanton contribution to the invariant squared mass is now

$$M^2 \approx \frac{k_\perp^2 + m_Q^2}{x\bar{x}} + 2P^+ P_-^- \approx \frac{k_\perp^2 + m_Q^2}{x\bar{x}} + 2M \left( \frac{4\kappa}{N_c \rho} \right) \mathbf{H}(\tilde{\xi}_x) \equiv \frac{k_\perp^2 + m_Q^2}{x\bar{x}} + 2MV_C(\xi_x) \quad (60)$$

which is an iterative equation for the mass  $M$ .  $\mathbf{H}(\xi_x)$  admits the short and large distance limits

$$\begin{aligned} \mathbf{H}(\tilde{\xi}_x) & \approx + \left( \frac{\pi^3}{48} - \frac{\pi^3}{3} J_1(2\pi) \right) \tilde{\xi}_x^2 + \left( -\frac{\pi^3(438 + 7\pi^2)}{30720} + \frac{J_2(2\pi)}{80} \right) \tilde{\xi}_x^4, \\ \mathbf{H}(\tilde{\xi}_x) & \approx -\frac{2\pi^2}{3} (\pi J_0(\pi) + J_1(\pi)) + \frac{C}{\tilde{\xi}_x^P}. \end{aligned} \quad (61)$$

## VI. SPIN INTERACTIONS ON THE LIGHT FRONT

To construct the spin-dependent interactions on the light front, we apply the general construction by Eichten and Feinberg [28] to the slated Wilson loop shown in Fig. 1 in Euclidean signature, followed by the analytical continuation  $\theta \rightarrow -i\chi$  to Minkowski signature. For that, we first need the expansion of the heavy-quark propagator shown as a straight line in leading order or  $1/m_Q^0$ , at next-to-next-to-leading order.

### A. Heavy-quark reduction

The heavy quark expansion of a Dirac fermion of mass  $m_Q$  with fixed velocity in an arbitrary gauge field is best achieved using the Foldy-Wouthuysen transformation on the relativistic fermion propagator,

$$e^{-i\frac{\not{p}_\perp}{2m_Q}} \frac{1}{i\not{D} - m_Q} e^{-i\frac{\not{p}_\perp}{2m_Q}} \quad (62)$$

with  $i\not{D} = i\not{d} + \not{A}$  and  $\not{D}_\perp = \not{D} - \not{v} \cdot \not{D}$  satisfying  $[\not{D}_\perp, \not{v}]_+ = 0$ . We will refer to  $v_\mu$  the two-dimensional light-conelike velocity along the two-dimensional light-conelike coordinate  $x_+$  in Euclidean signature, and to  $v_{\perp\mu}$  its orthogonal velocity along the two-dimensional light-conelike coordinate  $x_-$  also in Euclidean signature,

$$\begin{aligned} v_\mu & = (\mathbf{0}_\perp, \sin\theta, \cos\theta), \\ v_{\perp\mu} & = (\mathbf{0}_\perp, -\cos\theta, \sin\theta), \end{aligned} \quad (63)$$

with  $x_+ = v \cdot x$  and  $x_- = v_\perp \cdot x$ . These light-conelike Euclidean coordinations (lower indices) are not to be confused with the Minkowski light-cone coordinates  $x^\pm = x^0 \pm x^3$  (upper indices). With this in mind, and to order  $1/m_Q^2$  the heavy quark propagator is

$$\frac{1}{iv \cdot D} - \frac{1}{iv \cdot D} \left( \frac{1}{2m_Q} (i\not{D}_\perp)^2 - \frac{1}{4m_Q^2} (i\not{D}_\perp)(iv \cdot D)(i\not{D}_\perp) \right) \frac{1}{iv \cdot D}. \quad (64)$$

The bracket in (64) gives rise to a vertex insertion, which can be rearranged

$$\frac{1}{2m_Q} \left( (iD)^2 - \frac{1}{2} \sigma_{\mu\nu} F_{\mu\nu} \right) - \frac{1}{4m_Q^2} (i\sigma_{\alpha\nu} iD_\alpha v_\mu F_{\mu\nu} + iD_\nu v_\mu F_{\mu\nu}) \quad (65)$$

with  $\sigma_{\alpha\nu} = \frac{1}{2i} [\gamma_\alpha, \gamma_\nu]$ . In (65) we have dropped all terms that vanish on-shell, i.e.  $v \cdot D Q_v = 0$  with  $Q_v$  the heavy quark field. When inserted on a straight Wilson line, (65) produces the spin corrections up to order  $1/m_Q^2$ .



Note that in the Dirac representation  $\sigma_{4i}$  is off-diagonal. The electric contribution mixes particles and antiparticles. It does not contribute when inserted on a straight Wilson line defined as

$$\begin{aligned} \mathbf{W}(y, x) &= \langle y_+ | \frac{1}{v \cdot D} | x_+ \rangle \delta(\mathbf{x} - \mathbf{y}) \\ &= \mathbf{P} e^{i \int_{x_+}^{y_+} A \cdot dz} \theta(y_+ - x_+) \delta(\mathbf{x} - \mathbf{y}) \end{aligned} \quad (66)$$

with the ordering along  $x_+$  and the shorthand notations

$$\begin{aligned} x_\mu &= (\mathbf{x}_\perp, x_-, x_+) \equiv (\mathbf{x}, x_+), \\ y_\mu &= (\mathbf{y}_\perp, y_-, y_+) \equiv (\mathbf{y}, y_+). \end{aligned} \quad (67)$$

### B. Slated Wilson loop dressed with fields

The undressed Wilson loop in the resummed instanton vacuum is

$$\langle \mathbf{1}_\theta \rangle = \langle \mathbf{W}(\theta, 0_\perp) \mathbf{W}^\dagger(\theta, b_\perp) \rangle_C \approx e^{-Z_+ V_C(\xi_\theta)} \quad (68)$$

with

$$\xi_\theta = (\cos^2 \theta b_3^2 + b_\perp^2)^{\frac{1}{2}} \quad (69)$$

and where  $V_C(\xi_\theta) \rightarrow V_C(\xi_x)$  follows by analytical continuation  $\theta \rightarrow -i\chi$ . The spin dressed Wilson loop to order  $1/m_Q^2$  follows by inserting the corrections (64) on the Wilson lines

$$\begin{aligned} \langle \mathbf{1}_\theta \rangle \delta_{12} &+ \left( + \frac{i}{4m_{Q1}^2} \int_{-\frac{1}{2}Z_+}^{+\frac{1}{2}Z_+} dz_+ [\sigma_{1\alpha\nu} v_\mu \langle F_{\mu\nu}(x_1, z_+) iD_\alpha(x_1, z_+) \mathbf{1}_\theta \rangle + 1 \leftrightarrow 2] \right. \\ &+ \frac{1}{4m_{Q1}^2} \int_{-\frac{1}{2}Z_+}^{+\frac{1}{2}Z_+} dz_+ \int_{-\frac{1}{2}Z_+}^{+\frac{1}{2}Z_+} dz'_+ [\langle \sigma_{1\mu\nu} F_{\mu\nu}(x_1, z_+) (iD)^2(x_1, z'_+) \mathbf{1}_\theta \rangle + 1 \leftrightarrow 2] \\ &+ \frac{1}{8m_{Q1}m_{Q2}} \int_{-\frac{1}{2}Z_+}^{+\frac{1}{2}Z_+} dz_+ \int_{-\frac{1}{2}Z_+}^{+\frac{1}{2}Z_+} dz'_+ [\langle \sigma_{1\mu\nu} F_{\mu\nu}(x_1, z_+) (iD)^2(x_2, z'_+) \mathbf{1}_\theta \rangle \\ &+ \langle (iD)^2(x_1, z_+) \sigma_{2\mu\nu} F_{\mu\nu}(x_2, z'_+) \mathbf{1}_\theta \rangle \\ &\left. - \frac{1}{2} \langle \sigma_{1\mu\nu} F_{\mu\nu}(x_1, z_+) \sigma_{2\alpha\beta} F_{\alpha\beta}(x_2, z'_+) \mathbf{1}_\theta \rangle \right) \delta_{12} \end{aligned} \quad (70)$$

after dropping the terms that vanish on-shell, the terms that vanish by parity after averaging in the presence of the undressed Wilson loop, and those with no contribution to the spin-dependent potentials. In (70) we have labeled the quark masses for a general Wilson loop with unequal masses, and used the shorthand notation

$$\delta_{12} = \delta(\mathbf{x}_1 - \mathbf{y}_1) \delta(\mathbf{x}_2 - \mathbf{y}_2).$$

Throughout, the affine integration parameters  $z_+, z'_+$  in (70) are proper times. The conversion to ordinary times  $(z_+, z'_+) \rightarrow (z_+, z'_+)/\gamma_E$  amounts to extra Lorentz contraction factors of  $1/\gamma_E = \sqrt{1 + \dot{x}_E^2}$  in Euclidean signature, that will be added at the end by inspection.

### C. Identities

To simplify (70) we use the identities with slated Wilson lines (dropping the delta functions)

$$\mathbf{W}(x_+, y_+) \mathbf{W}(y_+, z_+) = \langle x_+ | \frac{1}{v \cdot D} | y_+ \rangle \langle y_+ | \frac{1}{v \cdot D} | z_+ \rangle = \langle x_+ | \frac{1}{v \cdot D} | z_+ \rangle = \mathbf{W}(x_+, z_+) \quad (71)$$

which is a property of the eikonalized and ordered Wilson line. More importantly, we have the identity

$$\begin{aligned} D_\nu(x_+) \mathbf{W}(x_+, y_+) - \mathbf{W}(x_+, y_+) D_\nu(y_+) \\ &= \langle x_+ | D_\nu \frac{1}{v \cdot D} - \frac{1}{v \cdot D} D_\nu | y_+ \rangle = \langle x_+ | \frac{1}{v \cdot D} [v \cdot D, D_\nu] \frac{1}{v \cdot D} | y_+ \rangle \\ &= \langle x_+ | \frac{1}{v \cdot D} (-iv_\mu F_{\mu\nu}) \frac{1}{v \cdot D} | y_+ \rangle = \int_{-\frac{1}{2}Z_+}^{+\frac{1}{2}Z_+} dz_+ \mathbf{W}(x_+, z_+) (-iv_\mu F_{\mu\nu})(z_+) \mathbf{W}(z_+, y_+). \end{aligned} \quad (72)$$

The end-point derivative of a Wilson line amounts to an insertion of a pertinent field strength (plaquette in a lattice form) along the line

$$v_\mu F_{\mu\nu} = v_4 F_{4\nu} + v_3 F_{3\nu} = \cos\theta F_{4\nu} + \sin\theta F_{3\nu}. \quad (73)$$

Finally, we have the large  $|z_+| \rightarrow \infty$  identity

$$\mathbf{W}(y, z_+; x, z_+) D_\alpha(x, z_+) \mathbf{W}(x, z_+; y, z_+) \rightarrow \partial_\alpha^y \quad (74)$$

as the fields are assumed to vanish at asymptotic  $z_+$ . A repeated use of (71)–(74) allows one to simplify (70).

#### D. First contribution in Eq. (70)

Consider the first contribution in (70) without  $1 \leftrightarrow 2$ ,

$$\int_{-\frac{1}{2}Z_+}^{+\frac{1}{2}Z_+} dz_+ \sigma_{1a\nu} v_\mu \langle F_{\mu\nu}(x_1, z_+) i D_\alpha(x_1, z_+) \mathbf{1}_\theta \rangle = \int_{-\frac{1}{2}Z_+}^{+\frac{1}{2}Z_+} dz_+ \sigma_{1a\nu} v_\mu \langle F_{\mu\nu}(x_1, z_+) \mathbf{1}_\theta \rangle i \partial_{1\alpha} \quad (75)$$

after using (72) forward and dropping a vanishing contribution by symmetry. Using again (72) backward we get

$$-\sigma_{1a\nu} \partial_{1\nu} \langle \mathbf{1}_\theta \rangle \partial_{1\alpha} \rightarrow -\epsilon_{ijk} \sigma_{1k} \partial_{1i} \langle \mathbf{1}_\theta \rangle \partial_{1j}. \quad (76)$$

Recall that  $\sigma_{4i}$  is off-diagonal in the Dirac representation. It drops out on a straight Wilson line, with no particle-antiparticle mixing. Hence the result

$$\frac{Z_+}{\gamma_E} e^{-Z_+ V_C(\xi_0)} \epsilon_{ijk} \sigma_{1k} (\partial_{1i} V_C(\xi_\theta)) \partial_{1j}, \quad (77)$$

with the additional Lorentz contraction factor in Euclidean signature, is restored.

The analytical continuation of (77) follows by taking  $\theta \rightarrow -i\chi$ ,  $\gamma_E \rightarrow \gamma \rightarrow \infty$ , with

$$\xi_\theta \rightarrow \xi_x = \sqrt{(\gamma b_3)^2 + b_\perp^2} \rightarrow \sqrt{(id/dx/M)^2 + b_\perp^2} \quad (78)$$

Hence,

$$\begin{aligned} \frac{1}{\gamma} \partial_{13} V_C(\xi_x) &= \frac{\partial V_C(\xi_x)}{\partial \gamma b_{13}} \rightarrow \frac{(id/dx_1)}{M \xi_x} V'_C(\xi_x), \\ \frac{1}{\gamma} \partial_{13} &= \frac{\partial}{\gamma \partial x_{13}} \rightarrow \frac{i p_{13}}{\gamma} = i s_1 m_{Q1} \end{aligned} \quad (79)$$

are the dominant contributions in (77) at large  $\gamma$ . The contribution to the squared mass operator is

$$M_{LS,C}^2 = 2M \left[ \frac{\sigma_1 \cdot (b_{12} \times s_1 \hat{3})}{4m_{Q1}} - \frac{\sigma_2 \cdot (b_{21} \times s_2 \hat{3})}{4m_{Q2}} \right] \frac{1}{\xi_x} V'_C(\xi_x) \quad (80)$$

after symmetrization, and dropping the higher order  $1/Mm_Q^2$  contribution. Here

$$b_{21} = (b_2 - b_1)_\perp \equiv b_\perp,$$

$s_1 = \text{sgn} p_{13}$  is the signum of the 3-momentum of particle 1 (sign of the helicity), and  $x_1$  refers to Bjorken  $x$  for particle 1 ( $x$  for particle and  $\bar{x}$  for antiparticle). This is the light-front form of the spin-orbit potential familiar from atomic physics.

#### E. Last contribution in Eq. (70)

Consider the spin-spin interaction in (70)

$$-\frac{1}{16m_{Q1}m_{Q2}} \int_{-\frac{1}{2}Z_+}^{+\frac{1}{2}Z_+} dz_+ \int_{-\frac{1}{2}Z_+}^{+\frac{1}{2}Z_+} dz'_+ [\langle \sigma_{1\mu\nu} F_{\mu\nu}(x_1, z_+) \sigma_{2\alpha\beta} F_{\alpha\beta}(x_2, z'_+) \mathbf{1}_\theta \rangle]. \quad (81)$$

Since  $\sigma_{4i}$  drops out of the straight Wilson line, the chief contribution in (81) is

$$-\frac{1}{4m_{Q1}m_{Q2}} \int_{-\frac{1}{2}Z_+}^{+\frac{1}{2}Z_+} dz_+ \int_{-\frac{1}{2}Z_+}^{+\frac{1}{2}Z_+} dz'_+ \sigma_{1i} \sigma_{2j} \langle B_i(x_1, z_+) B_j(x_2, z'_+) \mathbf{1}_\theta \rangle. \quad (82)$$

The magnetic correlation function in the presence of the Wilson loop  $\mathbf{1}_\theta$  can be rewritten as

$$\sigma_{1i} \sigma_{2j} \langle B_i(x_1, z_+) B_j(x_2, z'_+) \mathbf{1}_\theta \rangle = \sigma_{1\perp i} \sigma_{2\perp j} \langle B_{\perp i}(x_1, z_+) B_{\perp j}(x_2, z'_+) \mathbf{1}_\theta \rangle + \mathcal{O}\left(\frac{1}{\cos\theta}\right). \quad (83)$$

Here  $\vec{\sigma}_{1,2} = (\sigma_{\perp}, \sigma_3)_{1,2}$  with particle sublabeling 1,2, and the notation  $\perp = 1, 2$  (not to be confused with the projection orthogonal to  $v_{\mu}$  above). The longitudinal contribution of the magnetic field  $B_3$  ties to  $B_3 = -B_{-}/\cos\theta$ , with  $B_{-} = v_{\perp} \cdot B$  the component orthogonal to  $\mathbf{1}_{\theta}$ . After analytical continuation  $\theta \rightarrow -i\chi$  the contributions in  $1/\cos\theta$  in (81) are suppressed by  $\cos\theta \rightarrow \gamma_E \rightarrow \infty$

and will be dropped. This is expected since in the infinite momentum frame the transverse components of the gauge fields  $E_{\perp}, B_{\perp}$  dwarf the longitudinal ones  $E_3, B_3$ .

With this in mind, the result for the two-dimensional and transverse spin-spin potential prior to the analytical continuation is

$$\begin{aligned} & \frac{\sigma_{1\perp i} \sigma_{2\perp j}}{4m_{Q1} m_{Q2}} \left[ \left( \hat{b}_{\perp i} \hat{b}_{\perp j} - \frac{1}{2} \delta_{\perp ij} \right) \mathbb{V}_3(\xi_{\theta}, \theta) + \frac{1}{2} \delta_{\perp ij} \mathbb{V}_4(\xi_{\theta}, \theta) \right] \\ & = \frac{\sigma_{1\perp i} \sigma_{2\perp j}}{4m_{Q1} m_{Q2}} \left[ \lim_{Z_+ \rightarrow \infty} \frac{1}{Z_+ \langle \mathbf{1}_{\theta} \rangle \gamma_E^2} \int_{-\frac{1}{2}Z_+}^{+\frac{1}{2}Z_+} dz_+ \int_{-\frac{1}{2}Z_+}^{+\frac{1}{2}Z_+} dz'_+ \langle B_{\perp i}(x_1, z_+) B_{\perp j}(x_2, z'_+) \mathbf{1}_{\theta} \rangle \right] \end{aligned} \quad (84)$$

with the Lorentz contraction factor in Euclidean signature  $\gamma_E$  restored. Note the overall sign change in passing from the interaction (82) to the potentials (84). The analytical continuation in (84) will be carried explicitly below in the instanton vacuum. For general gauge fields, a numerical procedure needs to be developed.

### F. Remaining contributions in Eq. (70)

The remaining contributions in (70) are spin orbitlike. They can be simplified through a repeated use of the identities (71)–(74), and the observation that the longitudinal contributions of the gauge fields  $B_3 = -B_{-}/\cos\theta$  and similarly  $E_3 = -E_{-}/\cos\theta$  drop out after the analytical continuation and can be ignored.

The two cross spin-orbit contributions in the last line in (70),

$$\begin{aligned} & + \frac{1}{8m_{Q1} m_{Q2}} \left[ \int_{-\frac{1}{2}Z_+}^{+\frac{1}{2}Z_+} dz_+ \int_{-\frac{1}{2}Z_+}^{+\frac{1}{2}Z_+} dz'_+ \langle (\sigma_{1\mu\nu} F_{\mu\nu}(x_1, z_+) (iD)^2(x_2, z'_+) \mathbf{1}_{\theta}) \right. \\ & \left. + \langle (iD)^2(x_1, z_+) \sigma_{2\mu\nu} F_{\mu\nu}(x_2, z'_+) \mathbf{1}_{\theta} \rangle \right], \end{aligned} \quad (85)$$

can be simplified. First, we recall that  $\sigma_{4i}$  mixes particles and holes and does not contribute to the straight Wilson worldlines under consideration, so that the relevant contribution in (85) is

$$\begin{aligned} & + \frac{1}{4m_{Q1} m_{Q2}} \left[ \int_{-\frac{1}{2}Z_+}^{+\frac{1}{2}Z_+} dz_+ \int_{-\frac{1}{2}Z_+}^{+\frac{1}{2}Z_+} dz'_+ \langle (\sigma_{1k} B_k(x_1, z_+) (iD)^2(x_2, z'_+) \mathbf{1}_{\theta}) \right. \\ & \left. + \langle (iD)^2(x_1, z_+) \sigma_{2k} B_k(x_2, z'_+) \mathbf{1}_{\theta} \rangle \right]. \end{aligned} \quad (86)$$

Using the identities (72) and (74) we can rearrange the 12-integral in (86)

$$\begin{aligned} & \int_{-\frac{1}{2}Z_+}^{+\frac{1}{2}Z_+} dz_+ \int_{-\frac{1}{2}Z_+}^{+\frac{1}{2}Z_+} dz'_+ \langle \sigma_{1k} B_k(x_1, z_+) (iD)^2(x_2, z'_+) \mathbf{1}_{\theta} \rangle \\ & \approx 2\sigma_{1k} \int_{-\frac{1}{2}Z_+}^{+\frac{1}{2}Z_+} dz_+ \int_{-\frac{1}{2}Z_+}^{+\frac{1}{2}Z_+} dz'_+ \langle B_k(x_1, z_+) z'_+ v_{\mu} F_{\mu j}(x_2, z'_+) \mathbf{1}_{\theta} \rangle i\partial_{2j} \end{aligned} \quad (87)$$

where only the spin contributing terms are retained. In deriving (87) we used (74) to trade  $iD$  with  $i\partial_2$  at the edge of the Wilson line, followed by an integration by parts along  $z'_+$  using  $vD$  and then  $[vD, iD] = vF$ . With the analytical continuation in mind, the dominant contribution to the potential stems from  $j=3$  and  $v_4/\gamma_E = \cos\theta/\gamma_E \rightarrow 1$ , hence

$$\lim_{Z_+ \rightarrow \infty} \frac{1}{Z_+ \langle \mathbf{1}_{\theta} \rangle \gamma_E} \int_{-\frac{1}{2}Z_+}^{+\frac{1}{2}Z_+} dz_+ \int_{-\frac{1}{2}Z_+}^{+\frac{1}{2}Z_+} dz'_+ \langle B_k(x_1, z_+) z'_+ v_4 F_{43}(x_2, z'_+) \mathbf{1}_{\theta} \rangle \rightarrow \epsilon_{k3i} b_{21i} \frac{1}{\xi_x} \mathbb{V}'_2(\xi_x) \quad (88)$$

for the interaction, with  $b_{21} = -b_{12} \equiv b_{\perp}$ . If we recall the sign flip in passing from the interaction vertex to the potential, the 12 + 21 spin-orbit contribution to the squared mass operator is

$$\begin{aligned} M_{LS,12}^2 &= 2M \left( -\frac{1}{4m_{Q1}m_{Q2}} \left[ 2\sigma_{1k}\epsilon_{k3i}b_{21i} \frac{i\partial_{23}}{\gamma} + 1 \leftrightarrow 2 \right] \frac{1}{\xi_x} \mathbb{V}'_2(\xi_x) \right) \\ &= 2M \left( \left[ \frac{\sigma_2 \cdot (b_{12} \times s_1 \hat{3})}{2m_{Q2}} - \frac{\sigma_1 \cdot (b_{21} \times s_2 \hat{3})}{2m_{Q1}} \right] \frac{1}{\xi_x} \mathbb{V}'_2(\xi_x) \right). \end{aligned} \quad (89)$$

Using similar arguments, the spin-orbit contribution in the second line of (70) yields the dominant contribution to the interaction

$$\lim_{Z_+ \rightarrow \infty} \frac{1}{Z_+ \langle \mathbf{1}_\theta \rangle \gamma_E} \int_{-\frac{1}{2}Z_+}^{+\frac{1}{2}Z_+} dz_+ \int_{-\frac{1}{2}Z_+}^{+\frac{1}{2}Z_+} dz'_+ \langle \mathbf{B}_k(x_1, z_+) (z'_+ - z_+) v_4 F_{43}(x_1, z'_+) \mathbf{1}_\theta \rangle \rightarrow \epsilon_{k3i} b_{21i} \frac{1}{\xi_x} \mathbb{V}'_1(\xi_x) \quad (90)$$

with the corresponding 11 + 22 spin-orbit contribution to the squared mass operator

$$\begin{aligned} M_{LS,11}^2 &= 2M \left( -\left[ \frac{2}{4m_{Q1}^2} \sigma_{1k}\epsilon_{k3i}b_{21i} \frac{i\partial_{13}}{\gamma} + 1 \leftrightarrow 2 \right] \frac{1}{\xi_x} \mathbb{V}'_1(\xi_x) \right) \\ &= 2M \left( \left[ \frac{\sigma_1 \cdot (b_{12} \times s_1 \hat{3})}{2m_{Q1}} - \frac{\sigma_2 \cdot (b_{21} \times s_2 \hat{3})}{2m_{Q2}} \right] \frac{1}{\xi_x} \mathbb{V}'_1(\xi_x) \right). \end{aligned} \quad (91)$$

Below, we explicitly show how to evaluate  $\mathbb{V}_{1,2}(\xi_x)$  in the instanton vacuum. For general gauge fields, a numerical procedure needs to be developed, as we noted earlier for the spin-spin interaction (84).

(those due to the zero modes will be discussed below). They are related to the central electric potential  $V_C(\xi_x)$  in (60), since the induced spin correlators satisfy  $BB = EE$  and  $BE = \pm EE$  by self-duality.

## VII. LIGHT-FRONT HAMILTONIAN IN THE INSTANTON VACUUM

For the particular case of the instanton vacuum, these spin potentials are essentially generated by nonzero modes

### A. Spin-spin interaction

More specifically, the spin-spin interaction (84) with self-dual fields, reads

$$-\frac{\sigma_{1\perp i} \sigma_{2\perp j}}{4m_{Q1}m_{Q2}} \left[ \lim_{Z_+ \rightarrow \infty} \frac{1}{Z_+ \langle \mathbf{1}_\theta \rangle \gamma_E^2} \int_{-\frac{1}{2}Z_+}^{+\frac{1}{2}Z_+} dz_+ \int_{-\frac{1}{2}Z_+}^{+\frac{1}{2}Z_+} dz'_+ \langle E_{\perp i}(x_1, z_+) E_{\perp j}(x_2, z'_+) \mathbf{1}_\theta \rangle \right] \quad (92)$$

with here  $i, j = 1, 2$ . With this in mind, we now note that (73) amounts to

$$v_\mu F_{\mu i} = -R_{ij}(\theta) E_j \quad (93)$$

using again the self-duality for the instanton, with the rotation matrix

$$R(\theta) = \begin{pmatrix} \cos \theta & -\sin \theta \\ \sin \theta & \cos \theta \end{pmatrix} \rightarrow \gamma R = \gamma \begin{pmatrix} 1 & +i \\ -i & 1 \end{pmatrix} \quad (94)$$

and its analytical continuation. Note that for the anti-instanton which is anti-self-dual,  $R(\theta) \rightarrow R(-\theta)$  and  $R \rightarrow R^*$ . Inserting the inversion of (93) in (92) gives

$$-\frac{\sigma_{1\perp i} \sigma_{2\perp j}}{4m_{Q1}m_{Q2}} \left[ \lim_{Z_+ \rightarrow \infty} \frac{R_{im}(\theta) R_{jn}(\theta)}{Z_+ \langle \mathbf{1}_\theta \rangle \gamma_E^2} \int_{-\frac{1}{2}Z_+}^{+\frac{1}{2}Z_+} dz_+ \int_{-\frac{1}{2}Z_+}^{+\frac{1}{2}Z_+} dz'_+ \langle v_\mu F_{\mu m}(x_1, z_+) v_\nu F_{\nu n}(x_2, z'_+) \mathbf{1}_\theta \rangle \right]. \quad (95)$$

Using twice the identity (72) allows to simplify (95)



$$-\frac{\sigma_{1\perp i}\sigma_{2\perp j}}{4m_{Q1}m_{Q2}} \left[ \lim_{Z_+ \rightarrow \infty} \frac{-R_{im}(\theta)R_{jn}(\theta)\partial_m^1 \partial_n^2 \langle \mathbf{1}_\theta \rangle}{Z_+ \langle \mathbf{1}_\theta \rangle \gamma_E^2} \right]. \quad (96)$$

Recalling the overall sign flip in passing from the interaction to the potentials, the analytical continuation of (96) gives the instanton spin-spin contribution to the squared mass operator

$$\begin{aligned} M_{SS}^2 &= 2M \left( \frac{\sigma_{1\perp i}\sigma_{2\perp j}}{4m_{Q1}m_{Q2}} \left[ \left( \hat{b}_{12i}\hat{b}_{12j} - \frac{1}{2}\delta_{\perp ij} \right) \mathbb{V}_3(\xi_x) + \frac{1}{2}\delta_{\perp ij}\mathbb{V}_4(\xi_x) \right] \right) \\ &= 2M \left( \frac{\sigma_{1\perp i}\sigma_{2\perp j}}{4m_{Q1}m_{Q2}} [R_{im}R_{jn}\partial_{1m}\partial_{1n}V_C(\xi_x)] \right). \end{aligned} \quad (97)$$

Hence the relation of  $\mathbb{V}_{3,4}(\xi_x)$  to the central Coulomb potential  $\mathbb{V}_C(\xi_x)$  induced by instantons (anti-instantons) reads

$$\begin{aligned} \mathbb{V}_3(\xi_x) &= \frac{2b_\perp^2}{\xi_x^2} \mathbb{V}_C''(\xi_x), \\ \mathbb{V}_4(\xi_x) &= 0. \end{aligned} \quad (98)$$

In the instanton vacuum, the light-front spin-orbit potentials  $\mathbb{V}_{1,2}$  in (88)–(90), can be shown to be tied by the same identity as their counterparts in the rest frame [28], namely

$$\mathbb{V}_2(\xi_x) = \mathbb{V}_1(\xi_x) + V_C(\xi_x) \rightarrow \frac{1}{2}V_C(\xi_x) \quad (99)$$

with the rightmost result following in the instanton vacuum. Indeed, while on the light front  $\mathbb{V}_{2,4}(\xi_x)$  are no longer tied by the Bianchi identity (covariantized Lenz law), we note that the leading contributions in (88)–(90) match the rest frame contributions at  $\theta = 0$ . Therefore, the rest frame relation  $\mathbb{V}_2(R) = \frac{1}{2}V_C(R)$  in the instanton vacuum [28] (note the sign convention difference) carries to the light front  $\mathbb{V}_2(\xi_x) = \frac{1}{2}V_C(\xi_x)$ . This is not the case for  $\mathbb{V}_{3,4}(\xi_x)$  as we have shown.

## B. Light-front Hamiltonian

The sum of the spin contributions to the squared mass operator on the light front in the instanton vacuum is now explicit and of the form

$$\begin{aligned} M_{SD,I}^2(\xi_x, b_\perp) &= 2MV_{SD,I}(\xi_x, b_\perp) = 2M \left( \left[ \frac{\sigma_1 \cdot (b_{12} \times s_1 \hat{3})}{4m_{Q1}} - \frac{\sigma_2 \cdot (b_{21} \times s_2 \hat{3})}{4m_{Q2}} \right] \frac{1}{\xi_x} V_C'(\xi_x) \right. \\ &+ \left[ \frac{\sigma_1 \cdot (b_{12} \times s_1 \hat{3})}{2m_{Q1}} - \frac{\sigma_2 \cdot (b_{21} \times s_2 \hat{3})}{2m_{Q2}} \right] \frac{1}{\xi_x} \mathbb{V}_1'(\xi_x) \\ &+ \left[ \frac{\sigma_2 \cdot (b_{12} \times s_1 \hat{3})}{2m_{Q2}} - \frac{\sigma_1 \cdot (b_{21} \times s_2 \hat{3})}{2m_{Q1}} \right] \frac{1}{\xi_x} \mathbb{V}_2'(\xi_x) \\ &\left. + \frac{1}{4m_{Q1}m_{Q2}} \sigma_{1\perp i}\sigma_{2\perp j} \left[ \left( \hat{b}_{21i}\hat{b}_{21j} - \frac{1}{2}\delta_{\perp ij} \right) \mathbb{V}_3(\xi_x) \right] \right) \end{aligned} \quad (100)$$

with  $b_{21} = -b_{12} = b_\perp$  and  $s_{1,2}$  the signum of the velocity along the 3-direction (sign of the helicity). The contributions in (100) are in (80), (89), and (91). All spin potentials  $\mathbb{V}_{1,2,3}(\xi_x)$  are tied to the central potential  $\mathbb{V}_C(\xi_x)$  in the instanton vacuum, as in (98) and (99).

A key feature of the spin orbit contributions in (100) is that a flip of a spin, say  $\sigma_1$ , can be compensated by a flip in the sign of the helicity say  $s_1$  or  $s_2$ . This is reminiscent of the rest frame symmetry of the spin-orbit interactions, that show that a flip in the spin can be compensated by a flip in the angular momentum, thereby preserving the total angular momentum.

The light-front Hamiltonian in the instanton vacuum is the squared mass operator for a  $Q\bar{Q} \equiv Q_1Q_2$  pair, that

includes the free plus the central contribution in (60), and the spin contributions (100),

$$M^2 = \sum_{i=1,2} \frac{k_\perp^2 + m_{Qi}^2}{x_i} + 2M(V_C(\xi_x) + V_{SD,I}(\xi_x, b_\perp)) \quad (101)$$

with Bjorken  $x_{i=1,2}$  and satisfying  $x_1 + x_2 = 1$ . A detailed analyses of the spectrum and light-front wave functions following from (101) as applied to heavy and light mesons, with comparative estimates from perturbative one-gluon exchange and confinement, will be detailed in a sequel [11].

### VIII. SPIN INTERACTION FROM A STRING ON THE LIGHT FRONT

In the rest frame, the spin-dependent contributions emerging from the string were discussed by Buchmuller [29] and others [30,31]. Since the spin-spin interactions are short ranged, only the *self*-spin-orbit contributions survive at large separation  $R$ , where the string is active. Also, the electric flux tube is confined to the string, so the self-spin-orbit contribution is mostly induced by Thomas precession which is of *opposite sign* to the spin-orbit contribution from the standard Coulomb field.

More specifically, in the rest frame and at large separation only the self-spin-orbit potential survives [29–31],

$$M_{LS,\text{string}}^2 \approx 2M \left( \left[ \frac{\sigma_1 \cdot (b_{12} \times s_1 \hat{3})}{4m_{Q1}} - \frac{\sigma_2 \cdot (b_{21} \times s_2 \hat{3})}{4m_{Q2}} \right] (1-2) \frac{\sigma_T}{\xi_x} \right) \quad (103)$$

after using (99), and borrowing from the spin reduction structure in (80) and (91). As we noted in [14] (see Appendix B), the spin-orbit potential following from the analysis in [28] which we have followed (for both the instantons and string) is twice larger [32].

Finally, we note that on the light front, the sign of the string induced *formulas* spin-orbit in (103) is similar to the one expected from instantons in the dense regime, but opposite to the sign following from the perturbative Coulomb exchange, as originally noted in the rest frame in [29–31].

$$V_{LS,\text{string}}(R) \approx \left( \frac{\sigma_1 \cdot L_1}{4m_{Q1}^2} - \frac{\sigma_2 \cdot L_2}{4m_{Q2}^2} \right) \left( \frac{1}{R} V'_C(R) + \frac{2}{R} V'_1(R) \right) \\ \approx \left( \frac{\sigma_1 \cdot L_1}{4m_{Q1}^2} - \frac{\sigma_2 \cdot L_2}{4m_{Q2}^2} \right) (1-2) \frac{\sigma_T}{R} \quad (102)$$

with the convention for the orbital angular momenta  $L_1 = -L_2 = L$ . Here,  $V_C(R) = \sigma_T R$ , and  $V_1(R) \approx -V_C(R)$  from (99), since the *cross* spin-orbit potential being short ranged is expected to vanish at large  $R$ , i.e.  $V_2(R) \approx 0$ . On the light front, (102) can be recast, and its contribution to the squared mass operator is

### IX. SPIN-FLAVOR INTERACTIONS FOR LIGHT QUARKS

The spin-flavor interactions for light quarks are well understood in the rest frame. They involve chiefly the fermionic zero modes as they tunnel through instantons and anti-instantons. Because of the Pauli principle, only the zero modes with different flavors can undergo simultaneous tunneling, resulting in the famed 't Hooft interactions. For three flavors and in the zero size approximation, the 3-flavor interaction is repulsive and mostly active in the flavor singlet channel [33,34]

$$\mathcal{V}_{qqq}^{L+R} = \frac{G_{\text{Hooft}}}{N_c(N_c^2 - 1)} \left( \frac{2N_c + 1}{2(N_c + 2)} \det(UDS) \right. \\ \left. + \frac{1}{8(N_c + 1)} (\det(U_{\mu\nu} D_{\mu\nu} S) + \det(U_{\mu\nu} D S_{\mu\nu}) + \det(UD_{\mu\nu} S_{\mu\nu})) \right) + (L \leftrightarrow R) \quad (104)$$

with a strength

$$G_{\text{Hooft}} = \frac{n_{I+\bar{I}}}{2} \left( \frac{4\pi^2 \rho^3}{m_{Q\rho}} \right)^3 \quad (105)$$

and the short hand notations ( $Q \equiv U, D, S$ )

$$Q = \bar{q}_R q_L, \quad Q_{\mu\nu} = \bar{q}_R \sigma_{\mu\nu} q_L, \quad Q^a = \bar{q}_R \sigma^a q_L. \quad (106)$$

The 2-flavor  $ud$  interaction is attractive and follows by vacuum averaging the  $s$  contribution. It is also determinantal

$$\mathcal{V}_{qq}^{L+R} = \kappa_2 A_{2N} (\det(UD) + B_{2N} \det(U_{\mu\nu} D_{\mu\nu})) + (L \leftrightarrow R) \quad (107)$$

and attractive

$$\kappa_2 = 3! G_{\text{Hooft}} \langle \bar{s}_R s_L \rangle = 3 G_{\text{Hooft}} \langle \bar{s} s \rangle < 0,$$

$$A_{2N} = \frac{(2N_c - 1)}{2N_c(N_c^2 - 1)}, \quad B_{2N} = \frac{1}{4(2N_c - 1)}. \quad (108)$$

In the Weyl basis  $\sigma_{\mu\nu} \rightarrow i\eta_{\mu\nu}^a \sigma^a$  with the 't Hooft symbol satisfying  $\eta_{\mu\nu}^a \eta_{\mu\nu}^b = 4\delta^{ab}$ , and (104) can be simplified as

$$\mathcal{V}_{qq}^{L+R} = \kappa_2 A_{2N} (\det(UD) - 4B_{2N} \det(U^a D^a)) + (L \leftrightarrow R). \quad (109)$$

In the rest frame, (109) contributes an ultralocal interaction potential. In leading order in  $1/N_c$ , the potential in the  $U(1)$  or  $\eta'$  channel is

$$\frac{1}{2}\kappa_2 A_{2N} \frac{1}{2}(1 - \tau_1 \cdot \tau_2) \delta(\vec{x}_{12}) \quad (110)$$

with  $\vec{x}_{12} = \vec{x}_1 - \vec{x}_2$ . The corrections to (110) are nonrelativistic  $\nabla/m_Q$ .

The corresponding pair interaction on the light front in the eikonalized approximation can be written schematically as

$$\mathcal{V}_{12}^{L+R}(\tilde{\xi}_x) \rightarrow \frac{1}{2}\tilde{\kappa}_2 A_{2N} \frac{1}{2}(1 - \tau_1 \cdot \tau_2) \sigma_{\perp 1} \cdot \sigma_{\perp 2} \delta(\tilde{\xi}_x) \equiv \mathcal{V}_{\eta'}^{L+R} \delta(\tilde{\xi}_x) \quad (111)$$

in the  $\eta'$  channel, with  $\tilde{\kappa}_2 = \kappa_2/\rho^3$ . We dropped the spin-independent mass contributions; in writing (111) the delta function is assumed to depend only on the invariant 1D-like distance  $\tilde{\xi}_x$  defined in (58), in the local approximation. The alternative delta function

$$\delta(\tilde{\xi}_x) \rightarrow \delta(P^+ z^-) \delta(x_{\perp}/\rho),$$

which is 3D-like and local, will be discussed elsewhere. The flavor permutation inherent to the flavor singlet 't Hooft vertex is manifest in

$$1 - \mathbf{P}_{12} = \frac{1}{2}(1 - \tau_1 \cdot \tau_2) \quad (112)$$

with  $\mathbf{P}_{12}$  the flavor pair permutation operator. The spin-flip interaction  $\sigma_{\perp 1} \cdot \sigma_{\perp 2}$  remains on the light front in the near mass-shell limit, and flips the helicity of the incoming quark pair from L-left to R-right in the instanton contribution, and vice versa in the anti-instanton contribution. The corresponding interactions in the scalar and pseudo-scalar channels follow by Fierzing. There is no induced interaction by Fierzing in the vector and pseudovector channels. In particular, it is attractive in the pion channel and zero in the rho channel ( $N_c = 3$ ),

$$\begin{aligned} \mathcal{V}_{\pi}^{L+R}(\tilde{\xi}_x) &\approx \tilde{\kappa}_2 \delta(\tilde{\xi}_x), \\ \mathcal{V}_{\rho}^{L+R}(\tilde{\xi}_x) &\approx 0. \end{aligned} \quad (113)$$

For light quarks solely in the instanton vacuum, the light front mass operator (60) now reads

$$M^2 \approx \frac{k_{\perp}^2 + m_Q^2}{x\bar{x}} + 2M \left[ \left( \frac{4\kappa}{N_c \rho} \right) \mathbf{H}(\tilde{\xi}_x) + \mathcal{V}_P^{L+R}(\tilde{\xi}_x) \right], \quad (114)$$

where  $P$  refers to the nonvanishing Fierz contributions ( $P = \pi, \sigma, \pi_5, \sigma_5, \eta'$ ), with the constituent quark mass  $m_Q$

added. The instanton contributions and the constituent mass are of order  $\kappa$  in the packing fraction.

## X. THE PION ON THE LIGHT FRONT

The spontaneous breaking of chiral  $SU(N_f)_A$  symmetry is a fundamental and important phenomenon of nonperturbative QCD, much like confinement. The pion plays a very special role in it, being a Nambu-Goldstone (near massless) mode, a wave riding the vacuum quark condensate. The question then is, how does the pion emerge from (114) on the light front, with a *nonvanishing* constituent quark mass  $m_Q$ ? We will return to the pion wave function, including its quark spin-orbital wave functions, in our next publication. Here we give a qualitative description of the pion on the light front, in a vacuum randomly populated with only instantons and anti-instantons.

Let us start by noting that as  $M \rightarrow 0$ , then  $\tilde{\xi}_x \rightarrow |id/dx|/M\rho \gg 1$  in (58), and  $\mathbf{H}(\tilde{\xi}_x)$  is dominated by its large asymptotic constant in (61),

$$\mathbf{H}(\tilde{\xi}_x \gg 1) \rightarrow -\frac{2\pi^2}{3}(\pi J_0(\pi) + J_1(\pi)) \quad (115)$$

which should be removed because of confinement. With this in mind, and using (113) in the pion channel, we can rewrite (114) as

$$M^2 \approx \frac{M_{\perp}^2}{x\bar{x}} + 2M^2 \mathcal{V}_{\pi}^{L+R} \delta(M\tilde{\xi}_x)$$

with  $M_{\perp}^2 = k_{\perp}^2 + m_Q^2$  and  $\mathcal{V}_{\pi}^{L+R} = \tilde{\kappa}_2$ . Since

$$\delta(M\tilde{\xi}_x) = \rho \delta(|id/dx|)$$

we can formally solve for the squared mass operator in (115)

$$M^2 \approx (1 - 2\rho \mathcal{V}^{L+R} \delta(|id/dx|))^{-1} \frac{M_{\perp}^2}{x\bar{x}} \rightarrow \left[ \frac{1}{\sqrt{x\bar{x}}} (1 - 2\rho \mathcal{V}^{L+R} \delta(|id/dx|))^{-1} \frac{1}{\sqrt{x\bar{x}}} \right] M_{\perp}^2, \quad (116)$$

where the ordering ambiguity is fixed by symmetrization, to enforce hermiticity of  $M^2$ . Equation (116) admits a normalizable massless state

$$\varphi_\pi(x, b_\perp) = (6x\bar{x})^{\frac{1}{2}} \left( \frac{m_Q}{\sqrt{\pi}} K_0(m_Q |b_\perp|) \right) \quad (117)$$

with the normalization  $\int dx db_\perp \varphi_\pi^2(x, b_\perp) = 1$ . Indeed, the longitudinal part of (117) satisfies

$$\left[ \frac{1}{\sqrt{x\bar{x}}} (1 - 2\rho \mathcal{V}^{L+R} \delta(|id/dx|))^{-1} \frac{1}{\sqrt{x\bar{x}}} \right] \sqrt{x\bar{x}} = \left[ \frac{1}{\sqrt{x\bar{x}}} (1 - 2\rho \mathcal{V}^{L+R} \delta(0))^{-1} \right] 1 = 0.$$

When a small current mass  $m_q$  is added, the constituent mass shifts in leading order  $m_Q \rightarrow m_Q + m_q$ , and the pion becomes massive,

$$\begin{aligned} M_\pi^2 &= 2m_q m_Q \int_0^1 dx \frac{\varphi_\pi^2(x)}{x\bar{x}} + \mathcal{O}(m_q^2) \\ &= 12m_q m_Q + \mathcal{O}(m_q^2), \end{aligned} \quad (118)$$

as expected for a Goldstone mode. In the random instanton vacuum (RIV), the constituent mass  $m_Q$  follows from the breaking of chiral symmetry with explicitly

$$\langle \bar{q}q \rangle = -N_c m_Q / 2(\pi\rho)^2$$

(see for instance Eq. (84) in [14]), and (118) reduces to the GOR relation

$$M_\pi^2 = -2m_q \left[ \frac{\langle \bar{q}q \rangle}{f_\pi^2} \right] + \mathcal{O}(m_q^2). \quad (119)$$

The squared pion decay constant is identified as

$$f_\pi^2 = N_c / (\pi\rho)^2 / 12 = 1 / (2\pi\rho)^2. \quad (120)$$

The numerical value is surprisingly accurate, with  $f_\pi \sim 96$  MeV for  $\rho \sim \frac{1}{3}$  fm.

Note that in our case the pion—as a true Goldstone mode—is massless, even though the constituent quark mass

$m_Q \neq 0$ . The would-be pion in  $1 + 1$  dimensions becomes massless only in the large  $N_c \rightarrow \infty$  limit.

In Fig. 5 we show the longitudinal pion distribution amplitude in the random instanton vacuum on the light-front RIV (LFRIV) versus Bjorken  $x$ , following from (117) with  $\varphi_\pi^A(x) = \frac{x}{\pi} \sqrt{x\bar{x}}$  normalized as  $\int dx \varphi_\pi^A(x) = 1$ , at the low resolution of  $1/\rho$ . It is in good agreement with the pion DA in the random instanton vacuum RIV obtained in the rest frame, at the same resolution [35]. Both results are compared to the asymptotic pion DA of  $6x\bar{x}$  (dashed curve), and the lattice pion DA (green curved band) [36]. LFRIV is similar to the one derived using the Schwinger-Dyson construction [37], and identical to the pion longitudinal DA discussed using light-front holography [10].

The pion DA is driven by the spontaneous breaking of chiral symmetry, which is the same whether in the rest frame or in the light-cone frame, and as expected is not sensitive to the confinement mechanism. What is sensitive to confinement are the pion excited states, for instance the radial  $\pi(1300)$  excitation with assignments  $1^-(0^{+-})$  and higher, as we discussed earlier. In this case, the instanton contribution in (114) is only asymptotic and the role of confinement as in (23) is important. The relevant squared mass operator on the light front is now

$$M^2 \approx \frac{M_1^2}{x\bar{x}} + 2M[\text{spin}] + 2\sigma_T M\xi_x. \quad (121)$$

The short-range spin interactions due to the instantons' nonzero modes are given in Sec. VII.

## XI. CONCLUSIONS

We started this paper by discussing the basic problem of two massive relativistic quarks, connected by a classical Nambu-Gotto string. The problem was first set in the CM frame, in which the spectrum and the wave functions are readily obtained, by solving numerically in *Mathematica* (semiclassically or directly) a relativistic Klein-Gordon equation.

Then we considered the same problem on the light front (without spin effects), and derived the ensuing Hamiltonian. After turning it to a quadratic form (using the einbein trick), we defined an appropriate functional basis in which its diagonalization can be carried explicitly. It yields a meson spectrum that is consistent with the one from the rest frame, and with the expected and observed Regge behavior in terms

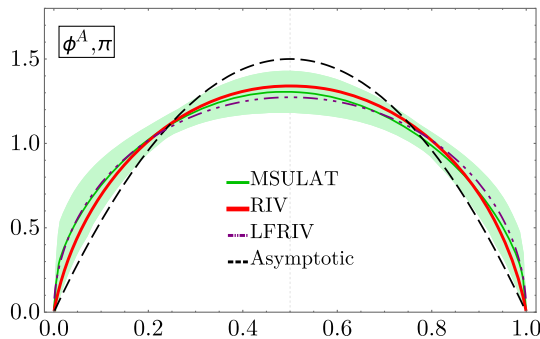


FIG. 5. RIV is the pion longitudinal DA from the instanton vacuum in the rest frame [35]; LFRIV is the pion DA from the instanton vacuum on the light front; Michigan State University lattice collaboration is the pion DA from the lattice [36]; the asymptotic pion DA of  $6x\bar{x}$  is shown for comparison.



of Regge slope. The Regge intercept turned out to be higher than the observed one, at least for the vector mesons we discussed.

The LFWFs of the low-lying states are obtained, as a function of the transverse momentum  $\rho = p_\perp$  and Bjorken  $x$ , see e.g. (34) for the ground state. To a good approximation, they are dominated by the lowest harmonic of the pertinent diagonalization set, a Gaussian in the  $p_\perp$  direction, and a  $\sin(\pi x)$  in the longitudinal direction.

A massless left-handed quark tunneling through an instanton emerges as a right-handed massless quark as a zero mode, a remarkable feature of a vector interaction. This is the essence of the dynamical breaking of chiral symmetry, which gives a running constituent mass. The collectivization of these zero modes is well understood in the rest frame, and yields the octet of massless Golstone modes. The QCD vacuum in the zero mode zone is “metallic,” with the scalar and vector mesons as weakly correlated “excitons.” Their orbitally excitations are sensitive to confinement.

The role of the nonperturbative vacuum structure on the light cone is best seen by noting that all hadron correlators on the light cone map onto a Wilson loop sloped at an angle  $\theta$  in Euclidean space, that analytically continues to  $-i\chi$  the rapidity in Minkowski space, a proposal we made long ago. An excited and confined meson, whether light or heavy, is characterized by a straight string with massive end points, to account for the scalar masses from the spontaneous breaking of chiral symmetry, plus current masses. In this sense all mesons behave democratically on the light cone.

The role of instantons and anti-instantons on the mesons in the light cone follows from the parallel Wilson lines before analytical continuation. Their effects fall into two categories: (i) the nonzero modes and (ii) the zero modes. The contribution of the nonzero modes can be explicitly calculated using the sloped Wilson loop, and then analytically continued to Minkowski space, giving rise to central and spin contributions to the mass operator. The contribution of the zero modes is still captured by the local form of the 't Hooft pair interaction, in addition to the constituent quark mass. We have explicitly assessed these contributions, and derived the pertinent mass operator in Minkowski signature. Modulo ordering ambiguities, it is iterative and nonlocal.

For a tightly bound pion where confinement is less active in a vacuum dominated by instantons, we have shown that this operator admits an exact Golstone mode on the light front, with the correct GOR relation and pion decay constant, and a universal and normalizable light-front DA. The latter is in good agreement with the one derived in the rest frame, using the quasi-DA construction.

The role of the spin effects on the light-light, heavy-light, and heavy-heavy mesons on the light front will be discussed next.

## ACKNOWLEDGMENTS

This work is supported by the Office of Science, U.S. Department of Energy under Contract No. DE-FG-88ER40388.

## APPENDIX A: KLEIN-GORDON EQUATION AND THE LOWEST MESON STATES

Now we return to the quantized version of the relativistic wave equation (5). Unlike the nonrelativistic Schrödinger equation, the energy  $E$  does not appear in it linearly, but is solvable. The problem with it is related with the solution behavior at large distances, beyond the turning point  $r > r_*$ . This is a textbook situation for the Schrödinger equation, where  $p^2$  changes sign and therefore  $p$  becomes imaginary. The correct solution decays exponentially in this region, hence the quantization condition  $\psi(r \rightarrow \infty) = 0$ .

The Klein-Gordon equation in this situation leads to a change of sign for  $\sqrt{p^2}$ , leading to complex  $p$ , so at large  $r$

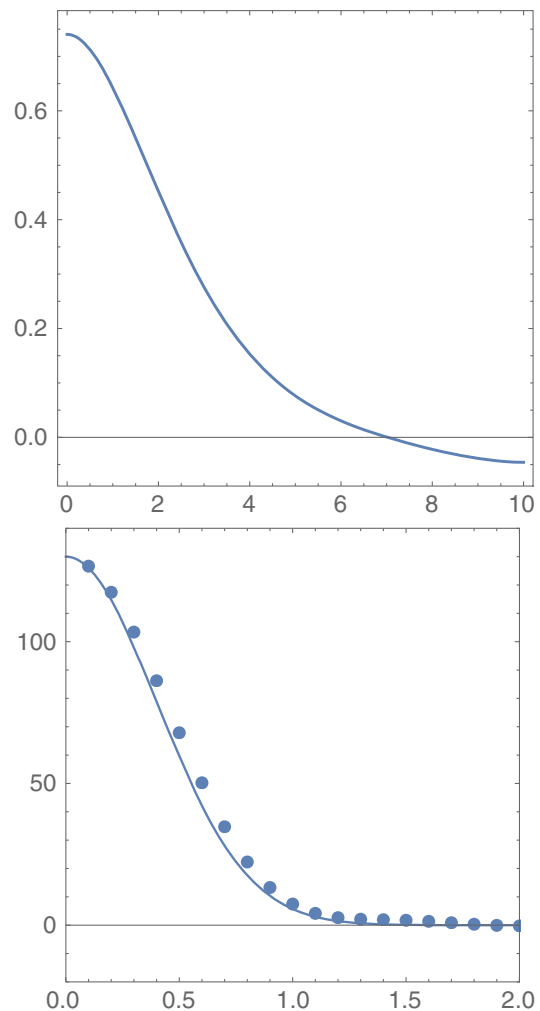


FIG. 6. The ground state wave function  $\psi_0(r)$  versus  $r(\text{GeV}^{-1})$  (top) and its Fourier transform  $\psi_0(p)$  (points, bottom) versus momentum  $p(\text{GeV})$ . The line is a Gaussian shown for comparison.

the solutions are oscillating with increasing frequency. Physically, this corresponds to the acceleration of produced quanta in a constant electric field, which obviously has no relation with the confining string problem we are after. This is at the origin of the Klein-paradox following from pair creation.

As an approximation, one may choose to consider the wave function only inside the “normal region”  $r < r_*$ , and use as a quantization condition the wave function vanishing at the turning point  $\psi(r_*) = 0$ .

For the constituent quark mass and string tension, the ground state wave function is shown in Fig. 6. The energy in the Klein-Gordon equation, corresponding to a half or reduced system, is 1.06 GeV, so the total mass is  $M_0 = 2.12$  GeV. Its Fourier transform (also calculated for  $r < r_*$ ) is shown in the lower plot for  $\psi_0(p)$ . For comparison we show a Gaussian fit with  $\langle p^2 \rangle^{1/2} = 0.33$  GeV.

## APPENDIX B: BASIS FUNCTIONS

### 1. The transverse oscillator

As explained in the text, we use the set of two-dimensional oscillator functions, with transverse momenta as the argument. One may either use a double set of standard one-dimensional oscillator functions in Cartesian coordinates, with quantum numbers  $n_x, n_y$ , or polar coordinates with quantum numbers  $n_\perp, m$ . We use the latter option. Although this is standard quantum mechanics, this set is less known. For completeness, we show how these functions are explicitly constructed and present several lowest functions explicitly for numerical use.

In Cartesian coordinates, the two-dimensional harmonic oscillator Hamiltonian and angular momentum along the  $z$  axis read

$$\begin{aligned} \hat{H} &= \frac{1}{2\mu} (\hat{p}_x^2 + \hat{p}_y^2) + \frac{\mu\omega^2}{2} (\hat{x}^2 + \hat{y}^2), \\ \hat{L}_z &= \hat{x}\hat{p}_y - \hat{y}\hat{p}_x. \end{aligned} \quad (\text{B1})$$

Since those operators commute, we will seek a common basis for both using the ladder construction. The operators reducing one quantum of oscillations are now defined as

$$a_R \equiv \frac{1}{\sqrt{2}}(a_x - ia_y), \quad a_L \equiv \frac{1}{\sqrt{2}}(a_x + ia_y), \quad (\text{B2})$$

in terms of the one-dimensional operators  $a_x, a_y$ . These operators change the eigenvalue of  $L_z$  or  $m$  by  $\mp 1$  unit. Their Hermitian conjugates change the eigenvalue by one more energy quantum. Furthermore,

$$\hat{L}_z/\hbar = a_R^\dagger a_R - a_L^\dagger a_L \quad (\text{B3})$$

and these two terms can be readily associated with the number of right- or left-rotating quanta. The energy is of course their sum, plus one from zero point oscillation

$$E/\hbar\omega = N_R + N_L + 1. \quad (\text{B4})$$

From now on we will use the notation  $n_\perp = N_R + N_L, m = N_R - N_L$  in reference to the two quantum numbers of the states.

The explicit wave functions can be expressed in polar coordinates  $\rho, \phi$  in which the reduction operators have the form

$$a_R = \frac{1}{2} e^{-i\phi} \left[ \beta\rho + \frac{1}{\beta} \frac{\partial}{\partial\rho} - \frac{i}{\beta\rho} \frac{\partial}{\partial\phi} \right], \quad (\text{B5})$$

$$a_L = \frac{1}{2} e^{i\phi} \left[ \beta\rho + \frac{1}{\beta} \frac{\partial}{\partial\rho} + \frac{i}{\beta\rho} \frac{\partial}{\partial\phi} \right], \quad (\text{B6})$$

where  $\beta = \sqrt{\mu\omega/\hbar}$ . Their Hermitian conjugates are obvious. Their actions on the ground state

$$\chi_{00} = \frac{\beta}{\sqrt{\pi}} \exp(-\beta^2 \rho^2/2) \quad (\text{B7})$$

yield all excited states. For example, the state with maximal orbital momentum has  $m$  right-rotating quanta  $m = N_R, N_L = 0$

$$\chi_{R^{NR}} = \frac{\beta}{\sqrt{\pi N_R!}} e^{iN_R\phi} (\beta\rho)^{N_R} \exp(-\beta^2 \rho^2/2) \quad (\text{B8})$$

and the minimal one  $m = -N_L$  follows using the change  $\phi \rightarrow -\phi, N_R \rightarrow N_L$ .

The main advantage of this basis set is that the orbital momentum  $\hat{L}_z$  commutes not only with  $H_0$  but with  $V$  as well: so  $m$  remains a good quantum number before we consider the spin-flip residual interactions. Here are the next two  $m = 0$  functions (after  $\chi_{00}$ ):

$$\chi_{RL} = \frac{\beta}{\sqrt{\pi}} \exp(-\beta^2 \rho^2/2) (\beta^2 \rho^2 - 1), \quad (\text{B9})$$

$$\chi_{RRL} = \frac{\beta}{\sqrt{2\pi}} \exp(-\beta^2 \rho^2/2) (2 - 4\beta^2 \rho^2 + \beta^4 \rho^4). \quad (\text{B10})$$

### 2. The longitudinal harmonics

Since the zeroth order Hamiltonian is quadratic in  $z^2 \sim \partial/\partial p_z$ , and  $p_z \equiv xP$ , the corresponding wave functions in  $[0, 1]$  are standing waves

$$f_{n_l}(x) \sim \sin(\pi(2n_l - 1)x) \quad (\text{B11})$$

that vanish at  $x = 0, 1$  and symmetric in  $x \leftrightarrow \bar{x} = 1 - x$ . In addition, we also have the constant wave function  $f_0(x) = 1$ , with the quantum number  $n_l = 0$ . Some matrix elements of this function are logarithmically divergent at the endpoints, in which case pertinent but physical cutoffs will be needed.

- [1] X. Ji, *Phys. Rev. Lett.* **110**, 262002 (2013).
- [2] J.-H. Zhang, J.-W. Chen, X. Ji, L. Jin, and H.-W. Lin, *Phys. Rev. D* **95**, 094514 (2017).
- [3] C. Alexandrou, K. Cichy, M. Constantinou, K. Jansen, A. Scapellato, and F. Steffens, *Phys. Rev. Lett.* **121**, 112001 (2018).
- [4] Y. Nambu and G. Jona-Lasinio, *Phys. Rev.* **122**, 345 (1961).
- [5] J. J. M. Verbaarschot and I. Zahed, *Phys. Rev. Lett.* **70**, 3852 (1993).
- [6] G. Montambaux, *Phys. Rev. B* **55**, 12833 (1997).
- [7] S. J. Brodsky and R. Shrock, *Proc. Natl. Acad. Sci. U.S.A.* **108**, 45 (2011).
- [8] S. J. Brodsky, C. D. Roberts, R. Shrock, and P. C. Tandy, *Phys. Rev. C* **85**, 065202 (2012).
- [9] X. Ji, *Nucl. Phys.* **B960**, 115181 (2020).
- [10] G. F. De Téramond and S. J. Brodsky, *Phys. Rev. D* **104**, 116009 (2021).
- [11] E. Shuryak and I. Zahed, following paper, *Phys. Rev. D* **107**, 034025 (2023).
- [12] E. Shuryak and I. Zahed, this issue, *Phys. Rev. D* **107**, 034026 (2023).
- [13] E. Shuryak and I. Zahed, this issue, *Phys. Rev. D* **107**, 034027 (2023).
- [14] E. Shuryak and I. Zahed, preceding paper, *Phys. Rev. D* **107**, 034023 (2023).
- [15] J. P. Vary, H. Honkanen, J. Li, P. Maris, S. J. Brodsky, A. Harindranath, G. F. de Téramond, P. Sternberg, E. G. Ng, and C. Yang, *Phys. Rev. C* **81**, 035205 (2010).
- [16] S. Jia and J. P. Vary, *Phys. Rev. C* **99**, 035206 (2019).
- [17] E. Shuryak, *Phys. Rev. D* **100**, 114018 (2019).
- [18] C. Mondal, J. Lan, K. Fu, S. Xu, Z. Hu, X. Zhao, and J. P. Vary, *SciPost Phys. Proc.* **10**, 036 (2022).
- [19] S. J. Brodsky, G. F. de Téramond, H. G. Dosch, and J. Erlich, *Phys. Rep.* **584**, 1 (2015).
- [20] A. Karch, E. Katz, D. T. Son, and M. A. Stephanov, *Phys. Rev. D* **74**, 015005 (2006).
- [21] E. Shuryak and I. Zahed, *Phys. Lett. B* **589**, 21 (2004).
- [22] J. Sonnenschein and D. Weissman, *J. High Energy Phys.* **08** (2014) 013.
- [23] I. Bars, *Nucl. Phys.* **B111**, 413 (1976).
- [24] I. Bars, *Phys. Rev. Lett.* **36**, 1521 (1976).
- [25] G. 't Hooft, *Nucl. Phys.* **B75**, 461 (1974).
- [26] H. J. Pirner, B. Galow, and O. Schlaudt, *Nucl. Phys.* **A819**, 135 (2009).
- [27] E. V. Shuryak and I. Zahed, *Phys. Rev. D* **62**, 085014 (2000).
- [28] E. Eichten and F. Feinberg, *Phys. Rev. D* **23**, 2724 (1981).
- [29] W. Buchmuller, *Phys. Lett.* **112B**, 479 (1982).
- [30] R. D. Pisarski and J. D. Stack, *Nucl. Phys.* **B286**, 657 (1987).
- [31] D. Gromes, *Z. Phys. C* **26**, 401 (1984).
- [32] A. Pineda and A. Vairo, *Phys. Rev. D* **63**, 054007 (2001); **64**, 039902(E) (2001).
- [33] S. Chernyshev, M. A. Nowak, and I. Zahed, *Phys. Rev. D* **53**, 5176 (1996).
- [34] E. Shuryak and I. Zahed, [arXiv:2102.00256](https://arxiv.org/abs/2102.00256).
- [35] A. Kock and I. Zahed, *Phys. Rev. D* **104**, 116028 (2021).
- [36] R. Zhang, C. Honkala, H.-W. Lin, and J.-W. Chen, *Phys. Rev. D* **102**, 094519 (2020).
- [37] C. D. Roberts, D. G. Richards, T. Horn, and L. Chang, *Prog. Part. Nucl. Phys.* **120**, 103883 (2021).